Cretaceous ultrapotassic magmatism from the Sava-Vardar Zone of the Balkans

Kristijan Sokol, Dejan Prelević, Rolf Romer, Milica Božović, Paul van den Bogaard, Elitsa Stefanova, Bojan Kostić, Nenad Čokulov

LITHOS 354-355 (2020) 105268

Contents lists available at ScienceDirect

LITHOS

journal homepage: www.elsevier.com/locate/lithos

Cretaceous ultrapotassic magmatism from the Sava-Vardar Zone of the Balkans

Kristijan Sokol [a], Dejan Prelević [a, b, *], Rolf L. Romer [c], Milica Božović [b], Paul van den Bogaard [d], Elitsa Stefanova [e], Bojan Kostić [a], Nenad Čokulov [a]

[a] University of Belgrade, Faculty of Mining and Geology, Đušina 7, 11000, Belgrade, Serbia
[b] Institute für Geowissenschaften, Johannes Gutenberg Universität, 55099, Mainz, Germany
[c] GFZ German Research Centre for Geosciences, Telegrafenberg, 14473, Potsdam, Germany
[d] Leibniz-Institut Für Meereswissenschaften, IFM-Geomar, Wischhofstr. 1–3, 24148, Kiel, Germany
[e] Geological Institute, Department of Mineralogy, Bulgarian Academy of Sciences, Acad. G. Bonchev-Str. Build. 24, 1113, Sofia, Bulgaria

ARTICLE INFO

Article history:
Received 26 July 2019
Received in revised form
23 October 2019
Accepted 28 October 2019
Available online 2 November 2019

Keywords:
Sava-Vardar zone
Mantle metasomatism
Cretaceous ultrapotassic rocks
Durbachite-vaugnerite series
Reconstruction geochemistry

ABSTRACT

Late Cretaceous global plate reorganization associated with the inception of counterclockwise rotation of Africa relative to Europe initiated in the Balkan region small-volume magmatism of diverse geochemical signature along the enigmatic Sava-Vardar Zone. We study a Late Cretaceous lamprophyric sill in Ripanj village near Belgrade to constrain this magmatic episode. The lamprophyre is characterized by high contents of Na, P, Fe and Al, and low contents of K, Ca and Mg. Its original nature (Na, K, Ca and Mg) is concealed by intense alteration (albitization of feldspar and partial chloritization of phlogopite) that erased the ultrapotassic affinity of the rocks and resulted in extremely low K/Na ratios. The recalculated chemical composition demonstrates that the rocks are ultrapotassic, with K_2O and MgO >3 wt % and $K_2O/Na_2O > 2$, and belong to the durbachite-vaugnerite series, i. e., the plutonic equivalents of minettes and kersantites.

Two phlogopite concentrates gave Ar–Ar ages of 86.80 ± 0.5 Ma and 86.90 ± 0.5 Ma. Our combined elemental and Sr–Nd–Pb isotope data ($^{87}Sr/^{86}Sr$ 0.70667–0.70677, $^{143}Nd/^{144}Nd$ 0.512426–0.512429, $^{206}Pb/^{204}Pb$ 18.82–19.13, $^{207}Pb/^{204}Pb$ 15.67–15.68, $^{208}Pb/^{204}Pb$ 38.92–39.19) for representative lamprophyric samples suggests magma derivation from a light rare earth elements (LREE) and K enriched, metasomatized mantle source. The content of LREE of the rocks is enriched, whereas heavy rare earth elements (HREE) is depleted. Rare earth elements (REE) of the whole rock and REE of diopside all indicate that garnet was present in their source.

There are two viable and mutually-excluding geodynamic scenarios for the Late Cretaceous magmatism in the Balkans: (i) If the Sava-Vardar ocean still existed in the Late Cretaceous and was subducted under the European plate with arc volcanism along the Apuseni-Banat-Timok-Panagyurishte-Srednjogorje belt, coeval magmatism in the Sava-Vardar Zone occurred in a fore-arc setting, and may be related to ridge subduction; (ii) If the Mesozoic ocean closed already during the Upper Jurassic or Lower Cretaceous, the Late Cretaceous volcanism within the Sava-Vardar Zone represents intra-continental volcanism associated with transtensional tectonics.

1. Introduction

The assessment of processes and parameters controlling magma formation and evolution during orogenesis ultimately provides information about the nature of the interplay between tectonics and magma generation and transport through the lithosphere. Previous geological, geochemical and tectonic studies (Pearce et al., 1990; Prelević et al., 2008) demonstrate that the transformation of an arc system into a collisional regime may be accompanied by magmatism either as a consequence of still active subduction, post-collisional lithosphere delamination associated with the orogenic collapse (Dewey et al., 1988) and/or tearing, segmentation and disruption of the subducted lithospheric slab (Prelević et al., 2015; Rosenbaum and Mo, 2011). Each major geodynamic episode during the collisional orogeny will lead to an array of diverse but

* Corresponding author. Institute für Geowissenschaften, Johannes Gutenberg Universität, 55099, Mainz. Germany.
E-mail address: dejan.prelevic@rgf.bg.ac.rs (D. Prelević).

https://doi.org/10.1016/j.lithos.2019.105268
0024-4937/

geochemically interrelated magmatic rocks, providing evidence for the nature of the geodynamic process itself. The geochemical variability of the magmatism reflects the involvement of different sources and melting regimes, and especially for post-collisional stages this may be misinterpreted as being related to arc volcanism due to activation of previously metasomatized lithospheric mantle or older crust carrying an arc signature (Pearce et al., 1990; Romer et al., 2001).

The Balkan Peninsula, an important segment of the Alpine-Himalayan collisional orogenic belt, includes several juxtaposed Phanerozoic orogens. The geology of its central axis is dominated by the Sava-Vardar Zone, a mega-suture zone (Cvetković et al., 2016; Pamić and Šparica, 1983; Schmid et al., 2008), which mirrors several episodes of the evolution of the Vardar branch(es) of the Neothethyan ocean, including its late Permian-Triassic opening, Jurassic intra-oceanic arc systems, Late Jurassic ophiolite obduction, Cretaceous ocean closure and Cenozoic post-collisional orogenic development (for further discussion, see Schmid et al. (2008) and Prelević et al. (2017)). From Jurassic initiation of subduction of Neotethyan oceanic lithosphere (Božović et al., 2013), the stepwise oceanic closure and collision was accomplished by Late Cretaceous, Oligocene, Miocene and Pliocene tectonic episodes related with geochemically diverse magmatism (Cvetković et al., 2004, 2010; 2014, 2016; Gallhofer et al., 2015; Prelević et al., 2017).

The Late Cretaceous tectonic episode is related with the waning stages of the Sava-Vardar ocean. It represents a puzzling issue (Schmid et al., 2008; Ustaszewski et al., 2009; Prelević et al., 2017), as it is unclear whether the whole oceanic segment was closed during Late Jurassic ophiolite obduction (e.g. Csontos and Vörös, 2004 and references therein) or some oceanic tracks persisted during the Late Cretaceous (e.g. Gallhofer et al., 2015 and references therein). This controversy reflects the complexity in determining the timing of the final closure of the Neothethyan ocean in the Balkans and the nature and age of deformation of sutured continental margins. For both issues, the origin of the Sava-Vardar Zone and its magmatic activity bear fundamental information about the pre- and post-collisional stages in the Balkans.

Here we study a unique ultrapotassic intrusion that is a part of recently established Late Cretaceous magmatic province along the Sava-Vardar Zone consisting of several magmatic intrusions (Prelević et al., 2017). Our new geochemical and geochronological data, in combination with recently established age constraints for other Cretaceous intrusions from the Balkans (Prelević et al., 2017) enable us to discuss viable models for the origin and geodynamic significance of this relatively short and enigmatic magmatic episode. Moreover, the spatial proximity and geochemical similarity of the Late Cretaceous and Cenozoic magmatism offers the possibility to study in detail the chemistry of their mantle source and its development through time.

2. Geology and magmatism within and in vicinity of the Sava-Vardar Zone

In the Balkans, the final stages of the Alpine orogeny are dominated by post-ophiolitic lithologies when the closure of the Tethyan ocean has taken place in the Cretaceous along the Sava-Vardar (suture) Zone (Karamata, 2006; Schmid et al., 2008; Ustaszewski et al., 2009). The Sava-Vardar Zone was defined by Kossmat (1924) as a zone that separates Dinarides and Helenides in the west, from the Serbo-Macedonian Massif to the east. It extends from the central Hungarian plain (Schmid et al., 2008; Ustaszewski et al., 2009) to Zagreb, then follows the river Sava, stretching over Fruška Gora to Belgrade where it bends southward in the direction of Skopje and Thessaloniki and eventually extends to the Izmir Zone of Turkey (Fig. 1a). The Sava-Vardar Zone comprises Upper-Cretaceous and Paleogene flysch sediments, Upper Cretaceous magmatic rocks, a tectonized Jurassic Ophiolitic mélange, as well as post-Mesozoic granites and volcanic formations. In the Late Cretaceous, the Sava-Vardar Zone either represents the forearc region of the youngest Neotethyan ocean that remained open until the latest Cretaceous (Toljić et al., 2018; Gallhofer et al., 2015; Schmid et al., 2008; Ustaszewski et al., 2009, 2010), or it delimits a diffuse tectonic boundary between Adria and Europe, which had already collided in the Late Jurassic (Csontos and Vörös, 2004; Prelević et al., 2017).

The Late Cretaceous volcanism within this zone is geochemically extremely variable, with intracontinental within-plate basalts near Klepa in North Macedonia (Prelević et al., 2017), moderately enriched tholeiitic and transitional basalts and rhyolites at Kozara in Bosnia and Herzegovina (Cvetković et al., 2014; Ustaszewski et al., 2009) and Papuk (Pamić et al., 2000), Moslavačka Gora (Starijaš et al., 2010), Prosara (Ustaszewski et al., 2010) and Požeška Gora (Pamić and Šparica, 1983; Pamić and Šiparica, 1988) in Croatia, lamprophyres from the Villány Mountains in southern Hungary (Nédli et al., 2010; Nédli and Tóth 2007), and an ultrapotassic intrusion near Ripanj in Serbia (Fig. 1b). The geodynamic framework of this volcanism is a matter of an ongoing debate (Cvetković et al., 2014; Prelević et al., 2017; Toljić et al., 2018). Especially puzzling is a relationship between the Late Cretaceous volcanism and $\geq$50 My younger Cenozoic magmatism occurring within the same zone, when the Balkans were a region of a considerable extension that triggered widespread magmatism of different geochemical affinity (Cvetković et al., 2004, 2016; Prelević et al., 2005, 2015).

The lamprophyric sill in the village of Ripanj near Belgrade is 100 m wide and in places up to 20 m thick (Fig. 2). It has steep and sharp contacts against the surrounding Cretaceous sediments of the so-called 'para flysch' sequence that represents a major post-ophiolite terrestrial sedimentary unit (Toljić et al., 2018). The green lamprophyre is relatively coarse-grained in the central parts and more fine-grained at the margins (Fig. 2).

3. Analytical methods

We analysed five lamprophyre samples from the Ripanj locality for major and trace elements by X-ray fluorescence (XRF) and inductively coupled plasma mass spectrometry (ICP-MS) and determined the Sr, Nd and Pb isotopic composition by thermal ionization mass spectrometry (TIMS). The samples used for isotope analysis were leached in diluted HCl before their isotopic compositions were determined. The analytical results of the whole-rock analyses are reported in Table 1. The full dataset on mineral composition is available as Supplementary Data.

Whole rock major element and Ni, Cr and Pb were determined by XRF spectrometry using a Philips MagiXPRO spectrometer on fused discs and pressed pellets at the University of Mainz. The rest of the trace elements were analysed by laser ablation (LA)-ICP-MS using an Agilent 7500ce ICP-MS system coupled with a New Wave UP-213 LA system at the University of Mainz. For that purpose, rock powders were melted to form homogeneous glass beads without any fluxing agent on an iridium strip heater in an argon atmosphere (Stoll et al., 2008). These glass beads were subsequently analysed by LA-ICP-MS. Details on measurement conditions have been reported by Božović et al. (2013) and Nehring et al. (2008).

Powders used for isotopic analysis were leached in 6N HCl overnight. This leaching should preferentially remove secondary minerals and, thus, the isotope signature associated with them. Samples were digested using HF in closed screw-top Savillex beakers on a hotplate for 4 days. Solutions were evaporated to near dryness, taken up in 2N HNO_3 to convert fluorides to nitrates and slowly dried again. The samples were redissolved in 6N HCl and once a clear solution was obtained split for Sr–Nd and Pb isotope

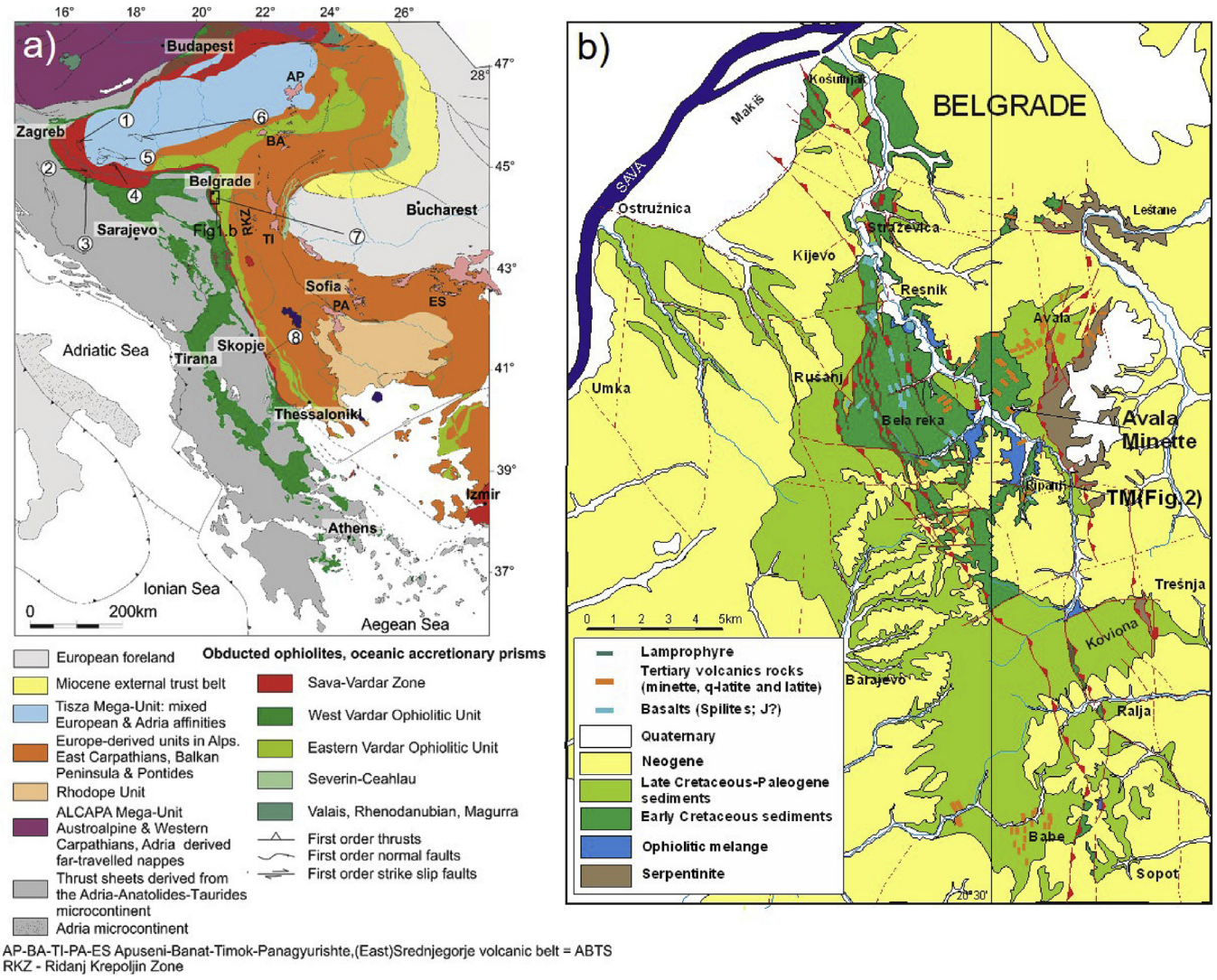

Fig. 1. a) Simplified geological map of the South–Eastern Europe (after Schmid et al., 2008). Numbered circles indicate discrete Late Cretaceous magmatic centres along the Sava-Vardar Zone mentioned in the text: 1) Moslovačka Gora; 2) Prosara; 3); Kozara; 4) Požeška Gora; 5) Papuk; 6) Villány Mts; 7) Ripanj and 8) Klepa. b) Simplified geological map of the area around Belgrade based on Toljić at al. (2018) and Geological Map of Yugoslavia 1:100.000 sheets Pančevo, Obrenovac, Smederevo and Belgrade. Ripanj locality where the lamprophyre sill crops out is depicted by the abbreviation TM (the old name of the quarry was Tešića Majdan). Avala minette represents an Oligocene lamprophyric sill (Prelević et al., 2005) in the vicinity of the studied Ripanj (TM) lamprophyre.

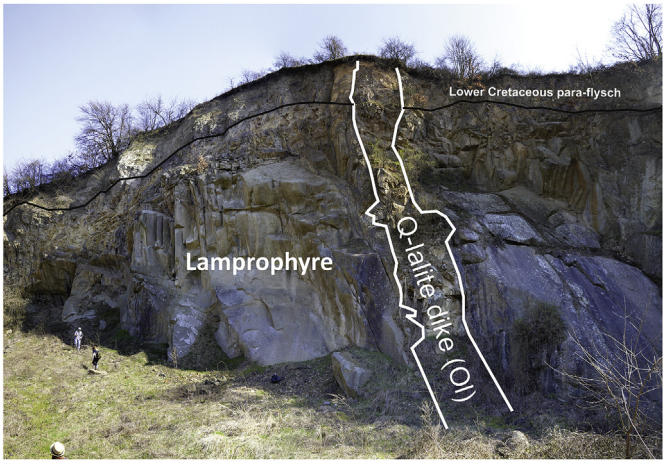

Fig. 2. Outcrop photo from the Ripanj quarry (Tešića Majdan) showing the Late Cretaceous lamprophyre (sill?) intruding into Early Cretaceous para-flysch: The Oligocene latite (K–Ar 25 Ma; Vasković, 1990) cuts these two units.

analysis. Sr, Nd, and Pb were separated using standard ion-exchange procedures (Romer et al., 2001). Special care was taken to remove Ba from the REE fraction (using an additional washing step with 2.5N HNO_3) to avoid interferences of BaO on mass ^{146}Nd. Sr and Nd isotope compositions were measured on a TRITON multi-collector thermal ionization mass spectrometer at GFZ German Research Centre for Geosciences (Potsdam) using Ta single and Re double filaments, respectively, operated in dynamic multi-collection mode. During the measurement period, NBS-987 Sr-reference material and the La Jolla Nd-standard yielded average $^{87}Sr/^{86}Sr$ and $^{143}Nd/^{144}Nd$ values of 0.710270 ± 14 (2σ of 18 measurements) and 0.511850 ± 7 (2σ of 11 measurements), respectively. The Pb isotopic composition was measured on a TRITON multi-collector thermal ionization mass spectrometer at GFZ German Research Centre for Geosciences (Potsdam) using single Re filaments and static multi-collection. Instrumental fractionation was corrected with 0.1% per atomic mass units (a.m.u.) as determined from the long-term reproducibility of Pb reference material NBS-981. Accuracy and precision of reported Pb isotope ratios is better than 0.1% at the 2σ level of uncertainty. For three samples,

Table 1
Major (wt %), trace element (ppm) concentrations and isotopic composition of the Late Cretaceous Ripanj lamprophyre, Serbia.

Sample	06TM01	06TM02	06TM03	06TM04	TM01/3	06TM02 Phlogopite
SiO_2	49.1	48.4	47.9	50.7	50.7	
TiO_2	1.3	1.1	1.3	1.2	1.2	
Al_2O_3	17.3	16.3	17.2	16.9	16.7	
Fe_2O_3	7.6	8.4	7.8	8.5	8.7	
MnO	0.2	0.1	0.2	0.1	0.1	
MgO	4.0	6.4	4.2	4.8	4.9	
CaO	5.5	7.7	6.3	6.4	6.7	
Na_2O	6.6	4.1	6.0	4.9	5.0	
K_2O	0.6	2.2	0.9	2.2	1.8	
P_2O_5	0.5	0.4	0.6	0.5	0.4	
LOI	6.7	4.5	7.3	3.5	3.2	
	99.4	99.5	99.4	99.7	99.4	
WR data (ppm) LAM-ICP-MS on glass beads Mainz						
Li	47.4	42.0	53.8	45.0	33.7	
Sc	13.6	23.3	12.9	11.8	8.9	
V	140	73.1	129	120	89.9	
Cr	34.9	28.8	31.3	29.4	22.1	
Ni	23.4	37.9	20.6	19.1	14.7	
Y	25.9	18.9	21.7	21.1	15.9	
Zr	347	321	278	278	208	
Nb	26.4	26.3	22.7	21.4	16.4	
Cs	0.358	0.282	0.298	0.288	0.218	
Ba	274	882	1387	206	137	
La	101	61.5	86.6	82.1	62.7	
Ce	170	113	160	168	165	
Pr	18.6	12.8	17.5	18.3	18.1	
Eu	2.87	2.18	2.64	2.81	2.75	
Gd	7.47	6.60	7.09	6.16	4.85	
Tb	0.927	0.755	0.879	0.764	0.602	
Dy	5.11	3.52	4.93	4.23	3.35	
Ho	0.927	0.626	0.905	0.769	0.611	
Er	2.43	1.66	2.26	2.08	1.56	
Tm	0.349	0.236	0.310	0.293	0.219	
Yb	2.24	1.49	1.77	1.78	1.34	
Lu	0.331	0.224	0.257	0.261	0.196	
Hf	7.60	7.31	5.93	6.01	4.51	
Ta	1.70	1.62	1.30	1.33	1.00	
Rb	15.1	53.7	28.5	14.8	14.5	
Sr	351	1389	417	304	256	
Sm	10.4	7.8	9.8	10.3	10.1	
Nd	68.6	46.0	63.9	67.4	66.2	
Pb	6.78	8.01	10.6	7.72	4.33	
Th	24.9	11.8	21.3	20.5	14.8	
U	5.16	5.03	5.21	5.17	5.50	
WR data (ppm) ICP-MS - leached samples						
Rb	18.9		29.2	33.3		
Sr	297		320	999		
Sm	2.35		2.61	4.56		
Nd	12.6		14.5	28.4		
Pb	2.16		4.29	1.89		
Th	14.8		14.8	8.55		
U	4.55		4.66	3.43		
WR data (ppm) Isotope dilution - leached samples						
Rb	16.7		24.7	23.5		
Sr	270		295	824		
Sm	2.30		2.53	4.48		
Nd	12.7		14.3	27.9		
Pb						2.05
Th						1.2
U						0.694
Age (Ma)	87	87	87	87	87	87
$^{87}Sr/^{86}Sr$	0.707388±5	0.706805±7	0.707536±5	0.706923±4	0.706863±7	
$^{87}Sr_{(T)}/^{86}Sr$	0.70717	0.70667	0.70724	0.70682	0.70666	
$^{143}Nd/^{144}Nd$	0.512503±4	0.512517±5	0.512508±4	0.512501±3	0.512519±5	
$^{143}Nd_{(T)}/^{144}Nd$	0.51244	0.51246	0.51245	0.51245	0.51247	
eNd (T)	−1.7	−1.3	−1.5	−1.6	−1.2	
$^{206}Pb/^{204}Pb$	19.411	18.821	18.977	19.479	19.128	18.733
$^{207}Pb/^{204}Pb$	15.681	15.669	15.659	15.688	15.681	15.639
$^{208}Pb/^{204}Pb$	39.572	38.924	39.111	39.421	39.190	38.774
$^{206}Pb/^{204}Pb_i$	17.59	18.27	18.02	17.89	18.01	18.44
$^{207}Pb/^{204}Pb_i$	15.59	15.64	15.61	15.61	15.63	15.62
$^{208}Pb/^{204}Pb_i$	37.58	38.50	38.11	38.10	38.20	38.60

the initial isotopic ratios of the leached powders were calculated using trace element contents determined by LA-ICP-MS or isotope dilution on aliquots of the same solutions used for determining the isotopic composition of Sr, Nd, and Pb. For two samples (analysed earlier) this was not possible and the contents of the unleached powders were used. The difference in parent-to-daughter element ratio is small and – given the young age of the samples – does not affect the recalculated values significantly.

$^{40}Ar/^{39}Ar$ increment heating experiments were conducted on two samples (Tm02bts and Tm02bt2) of phlogopite crystals separates at the GEOMAR tephrochronology Laboratory. The phlogopite crystals >0.5 mm were hand-picked from crushed and sieved splits and cleaned using an ultrasonic disintegrator. Afterwards, the crystals were etched in 15% hydrofluoric acid for 10 min. The dry samples were loaded in aluminum trays and irradiation cans that were wrapped in 0.7 mm cadmium foil and irradiated at the 5 MW reactor of the GKSS Reactor Central (Geesthacht, Federal Republic of Germany). $^{40}Ar/^{39}Ar$ age determinations were performed by fusing single crystals using laser-step heating. Purified gas samples were analysed using a MAP 216 series noble gas mass spectrometer. The measured Ar isotope ratios were corrected for mass discrimination, background and blank values. Neutron flux during irradiation was monitored using TCR sanidine (Taylor Creek Rhyolite, 27.92 Ma) (Dalrymple and Duffield, 1988) and an internal standard SAN6165 (0.470 Ma; Van den Bogaard, 1995). Vertical variations in J values were quantified by a cosine function fit. Lateral variations in J were not detected. Corrections for interfering neutron reactions on Ca and K were based on analyses of optical grade CaF_2 and high-purity K_2SO_4 salt crystals that were irradiated together with the samples. Ages derived from step-heating analyses are based on the plateau portions of the age spectra. Plateau regions generally comprise >50% of the ^{39}Ar released and more than three consecutive heating steps that yield the same ages (within 2σ).

The major element composition of minerals was determined by electron microprobe (JEOL JXA 8900RL) at the Department of Geosciences, University of Mainz, Germany, using wavelength-dispersive analysis and a range of natural and synthetic standards. The data were corrected using the CITZAF procedure; detection limits were between 0.01 and 0.07 wt %. Operating conditions were generally 15 kV (20 kV) accelerating voltage, 12 nA beam current, 1–5 μm beam diameter and 15–30 s counting time on peak. Synthetic and natural minerals were used for standardization. Back-scattered imaging was performed using a SEM, a model JEOL JSM-6610LV, at the University of Belgrade-Faculty of Mining and Geology.

Mineral trace element compositions were performed at the Geological Institute of the Bulgarian Academy of Sciences (GI-BAS, Sofia) by laser ablation inductively coupled plasma mass spectrometry (LA–ICP-MS) using laser ablation system New Wave UP193FX coupled with an ICP–MS PerkinElmer ELAN DRC-e. For these analyses, the laser spot diameter was 50-30 μm. The energy of laser ablation was 10 Hz and 10 J/cm^2, respectively. The SRM NIST 610 standard glass was used for calibration with Si and Ca as internal standards. US Geological Survey (USGS) reference glass BCR-2G was measured as an unknown after every tenth sample spot, and the results were in agreement with literature data.

4. Results

4.1. Petrography and classification

The Ripanj rocks are characterized by typical granular to weakly macrocrystic texture, with the mm-sized poikilitic phlogopite, diopside, plagioclase and orthoclase and abundant apatite (Figs. 3 and 4). The phlogopite grains are dominantly fresh showing subordinate chloritisation (Fig. 3). Similarly, diopside grains are slightly uralitized/chloritized in all samples (Fig. 3). In contrast, plagioclase grains are consistently albitized, and they are difficult to distinguish optically from alkali feldspar (Fig. 4). Whereas texture and morphology resemble plagioclase, optical properties are those of alkali feldspar, suggesting that the albite occupies the volume of former plagioclase. Similarly, orthoclase grains are intensely saussuritized and albitized as well, and only a few samples show remnants of fresh orthoclase (Fig. 4a).

The albitisation and sausuritization of feldspar strongly affect the chemical composition of the rocks, most importantly the alkali ratios and the extent of potassium enrichment. To reconstruct the original rock composition, we performed a thorough modal analysis, applying the point counting method using optical microscope images and scanned thin sections (Fig. 5). Using the image processing program ImageJ, we calculated the area distribution of the main minerals and calculated the modal abundance. For details, see the caption of Fig. 5. The reconstruction gave the following modal abundances: 52–60% feldspars, 20–25% diopside and 16–22% phlogopite. Combining BS images and WDS analyses, modal abundances show 24–27% orthoclase and 28–33% plagioclase (Supplementary Data). The modal mineral abundance in combination with average mineral composition was used to estimate the original whole rock major element contents (see below).

The modal analyses imply that the Ripanj rock represents a plutonic (coarse-grained granular) equivalent of phlogopite-lamprophyre. This is in accordance to generally accepted definitions (Rock, 1991) that lamprophyres are melanocratic hypabyssal igneous rocks with microporphyritic textures carrying hydrous mafic phenocrysts, with feldspar and other felsic minerals being restricted to the groundmass. Due to the presence of plagioclase in the holocrystalline phaneritic groundmass (Fig. 5), the Ripanj rocks may be classified as vaugnerite that represents the plutonic equivalent of kersantite (Le Maitre, 2002).

4.2. Mineral chemistry

Ripanj lamprophyre contains alkali feldspar that is intensely altered to a mixture of white mica (sericite) flakes and a clay-like material. There are, however, numerous fresh patches and grains demonstrating Carlsbad twinning (Fig. 4). On the other hand, plagioclase is universally pseudomorphed by Ca and K free albite (Fig. 4, Supplementary dataset).

Analysed clinopyroxene (CPX) from the Ripanj lamprophyric rocks are Ca–Mg–Fe pyroxenes (Morimoto, 1988). Their composition ranges between diopside and augite (only a few measurements are Cr rich) with major components in the range of En 38–45, Fs 10–14 and Wo 44–47. Clinopyroxene is characterized by relatively low TiO_2 (0.71–2.1 wt %) and moderate to high Al_2O_3 (3.1–7.1 wt %) contents. There is a systematic compositional change from relatively high MgO, medium to low Al_2O_3, low TiO_2 and high Cr_2O_3 (up to 0.3 wt %) cores towards more evolved outer rims having higher Al_2O_3, TiO_2 and lower Cr_2O_3 contents (Fig. 6a). Patchy or reverse zonation patterns are subordinate.

Using the Al vs Ti plot (Fig. 6b) we compare Ripanj clinopyroxene with the compositional fields of clinopyroxene from Italian potassium-rich lavas Perini and Conticelli (2002). For comparison, we plot the analyses of clinopyroxene from the Klepa alkaline within-plate basalts, which represent activity within the Sava-Vardar Zone that was broadly coeval with the Ripanj magmatism. The plots clearly demonstrate that clinopyroxene from the Ripanj lamprophyre is generally more alumina rich than clinopyroxene from Italian lamproitic lavas, but with the similarly low titanium contents. On the other hand, the Klepa clinopyroxene plots on an entirely different trend with consistently higher titanium and alumina concentrations for similar MgO contents (Fig. 6a and b).

The trace element composition of clinopyroxene

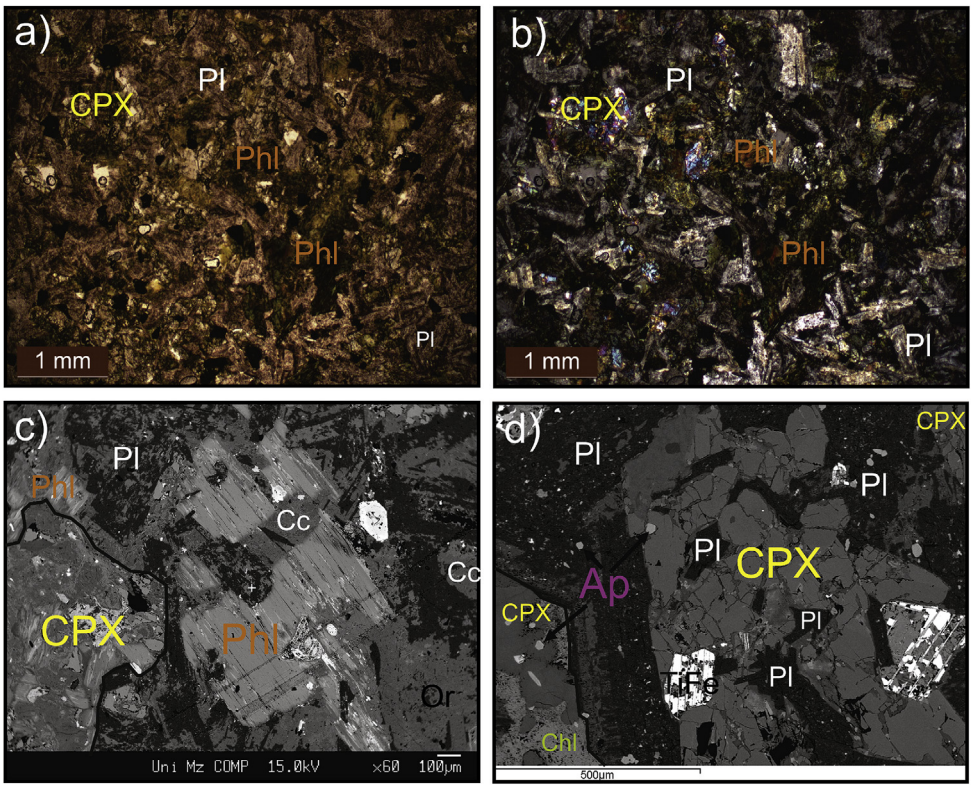

Fig. 3. Photomicrographs of representative samples of the Late Cretaceous Ripanj lamprophyre: a) Plane polarised light (PPL) image illustrating the ophitic texture of the rock, comprising of clinopyroxene and phlogopite grains in a coarse-grained groundmass consisting mainly of diopside-rich clinopyroxene, albite, and orthoclase. b) Crosse polarised light (XPL) image of the same area shown in a). c) and d) Back-scattered electron images of phlogopite (Phl) clinopyroxene (Cpx), plagioclase (Pl) and apatite (Ap). Abbreviations are from Kretz, 1983.

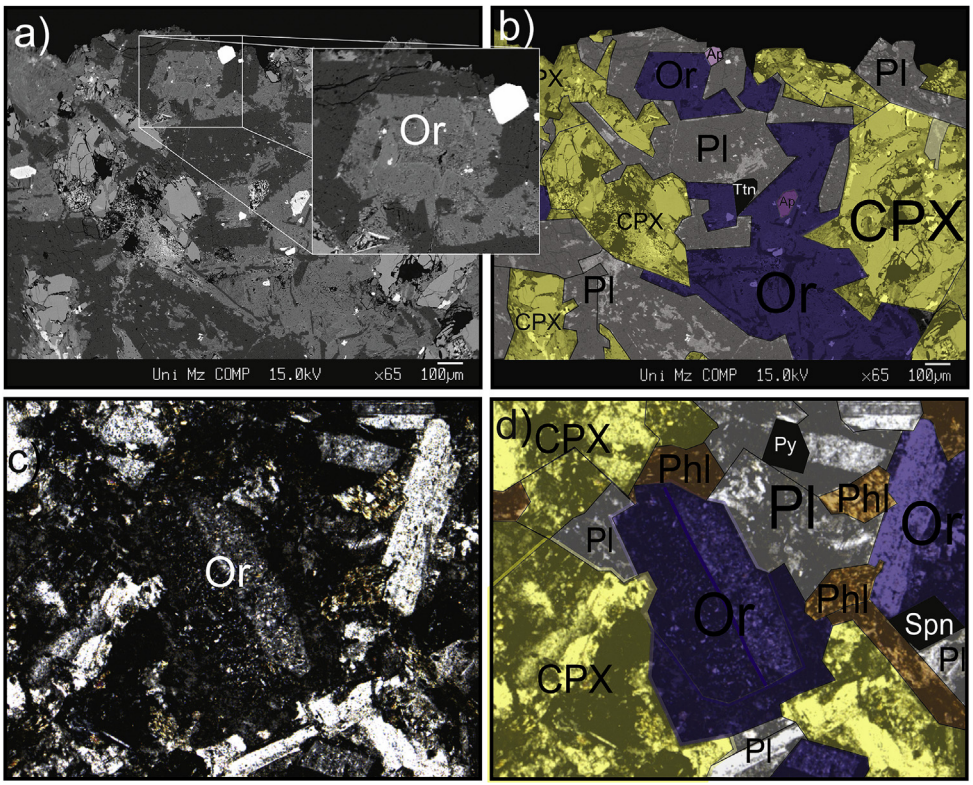

Fig. 4. Photomicrographs and back-scattered electron images of representative samples of the Late Cretaceous lamprophyre from Ripanj. a) and c) show the present mineralogy, b) and d) show the reconstructed mineral composition of the same samples. Inset in a) shows a detailed view of alkali feldspar (Or) alteration. Abbreviations are from Kretz, 1983.

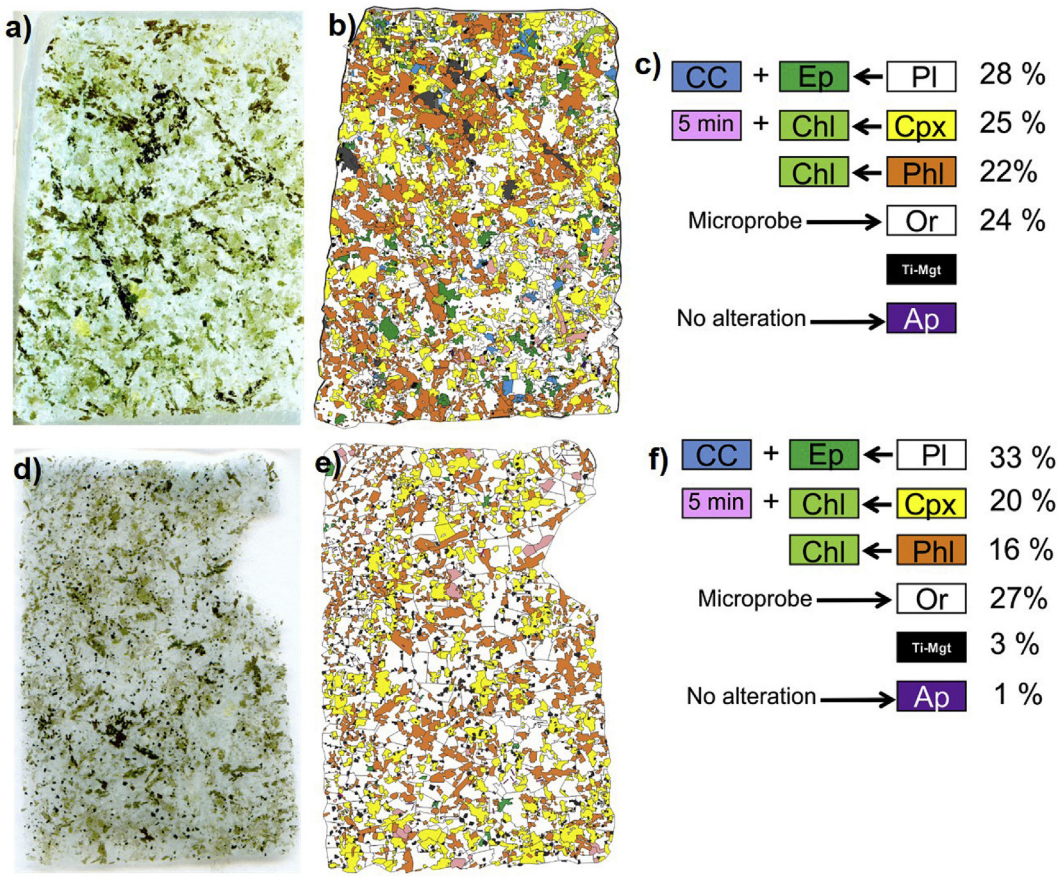

Fig. 5. Reconstruction of the original mineralogy of the Ripanj lamprophyre. a) and d) Thin sections 06TM02 and 06TM04. The dimension of the sections is 30 × 20 mm. b) and e) Reconstructed modal analysis of samples shown in a) and b). c) and f) The reconstruction of the original mineralogy bases on the alteration products of the four main rock-forming minerals. Plagioclase (Pl) (albitized) altered to epidote (Ep) and calcite (Cc), orthoclase (Or) altered to kaolinite (Kln) and sericite (Ser), phlogopite (Phl) altered to chlorite (Chl) and a titanium phase (Ti), and diopside (Cpx) altered to an assemblage of several minerals, including chlorite, calcite, sphene (Spn) or Ti-magnetite (Ti-Mgt), zoisite (Zo), and allanite (Al). These latter minerals are summarized as "5 min". Abbreviation are from Kretz (1983).

(Supplementary Data) does not show a substantial difference between different grains and samples. The REE patterns from several grains are subparallel (Fig. 6c) suggesting that clinopyroxene from the Ripanj lamprophyres has relatively homogeneous compositions reflecting a high degree of light to heavy rare earth element fractionation (LREE/HREE).

Micas from Ripanj lamprophyres are phlogopites (Deer et al., 1966, Fig. 7). Their compositions plot in the field of micas from calc-alkaline lamprophyres (CAL) in Al_2O_3 vs TiO_2 (Fig. 7a) and FeO diagrams (Mitchell and Bergman, 1991). The low Cr_2O_3 (0.02–0.05 wt %) contents and Mg# (68–75) indicate that phlogopite is quite evolved, in accordance with its late crystallization (poikilitic texture, Fig. 3). This conclusion is supported by relatively low K_2O contents (8.0–8.5 wt %) and high BaO concentrations (0.87–1.7 wt %). Moreover, Ripanj phlogopite has high concentrations of Na_2O (0.8–1.1 wt %), which is atypical for micas crystallized from mafic K-rich lavas. For comparison, phlogopite from Mediterranean lamproites typically has less than 0.6 wt % Na_2O (Fritschle et al., 2013).

Phlogopite from Ripanj lamprophyres has high to moderate contents of incompatible trace elements and LILE (Fig. 7b and c), with extreme Li contents up to 200 ppm. Higher Li enrichment is only known from lamproitic phlogopite from a single location (Jumilla in Spain; Fritschle et al., 2013). Phlogopite from Ripanj has high concentrations of Nb (up to 50 ppm) and Ta. Compared with phlogopite from Mediterranean lamproites, they have lower Ni contents, in accordance to their late crystallization.

To elucidate the possible source of mantle metasomatism, data on Ripanj phlogopite is compared with published data on Mediterranean lamproitic phlogopite whose trace element ratios were applied for mantle fingerprinting. Using ratios of similarly incompatible trace elements such as Cs/Rb and Zr/Nb (Fritschle et al., 2013) distinguished different types of metasomatic melts (Fig. 7b), including melts having contributions of recycled continental crust (Prelević et al., 2013) and alkaline basaltic precursor melts derived from the asthenosphere (Pilet, 2015). Despite relatively high Cs/Rb ratios and Li enrichment that may be interpreted as clear crustal fingerprint (Fritschle et al., 2013), Ripanj phlogopite is characterized by relatively low Zr/Nb ratios, which is not fully in line with that interpretation (Fig. 7b).

4.3. Whole rock geochemistry

The Ripanj lamprophyric rocks (raw data) have moderate bulk rock MgO (5–7 wt %) and relatively high SiO_2 (48–52 wt %) and Al_2O_3 (16–17 wt %) contents. The contents of CaO (4.5–6 wt %) and TiO_2 (1–1.2 wt %) are relatively low (Table 1). The low K_2O contents (0.6–2.2 wt %) are reversely correlated with very high Na_2O (5–6 wt %). Much lower K_2O contents and K_2O/Na_2O ratios than expected from their petrographic phlogopite-phyric composition in which phlogopite is obviously a liquidus phase, represents the most dramatic consequence of the spilitization. Comparison of the measured major element data with the reconstructed composition based on modal analyses shows that spilitization had the strongest effect on the amounts of K_2O and Na_2O, and their ratios (Fig. 8).

The HFSE and REE signature of the Ripanj lamprophyres

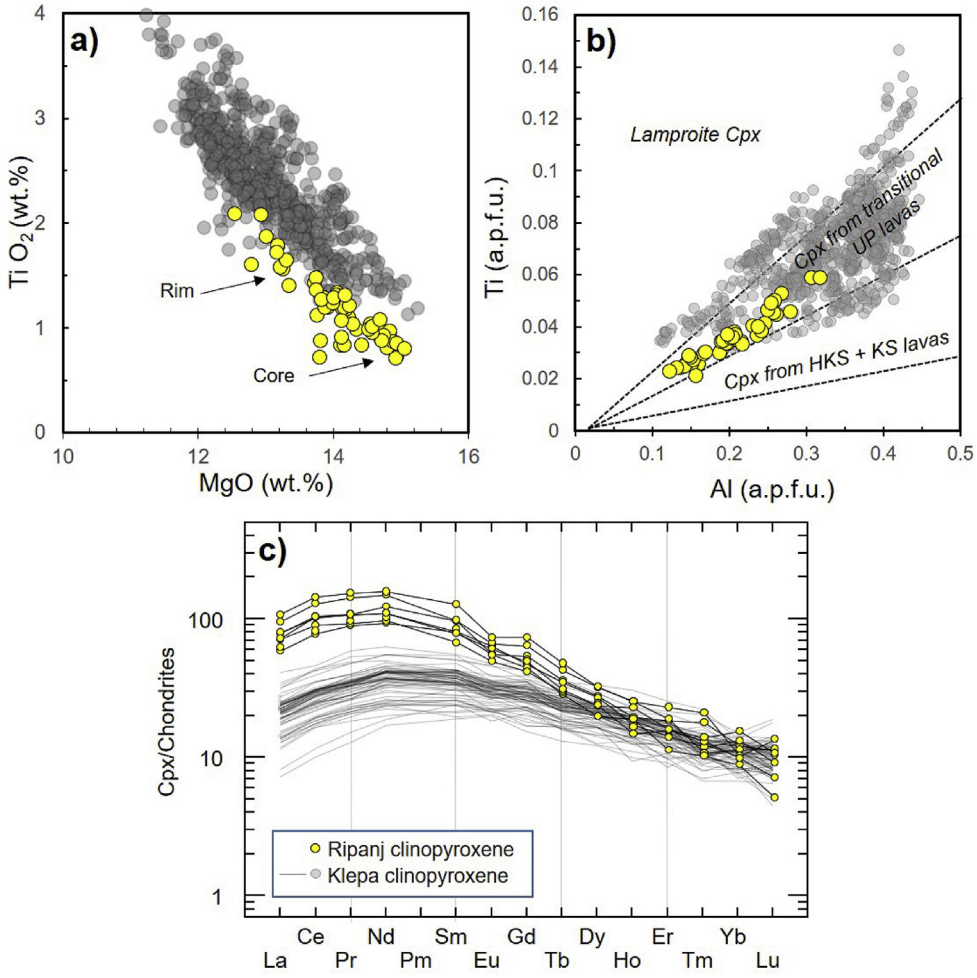

Fig. 6. a) Al vs Ti Atom per formula unit or (a.p.f.u.) and b) TiO_2 vs MgO for clinopyroxene phenocrysts. Yellow circles represent measurements from the Ripanj lamprophyre, the grey circles represent clinopyroxenes from Klepa basalts (Prelević et al., 2017). The field for lamproite clinopyroxene is from Mitchell and Bergman (1991); fields for clinopyroxene from the Italian volcanic province: high-potassium series (HKS), potassium series (KS) and transitional rocks are after Perini and Conticelli (2002) and references therein. c) Chondrite-normalized rare earth element patterns for representative clinopyroxene (diopside) crystals from the Ripanj lamprophyre (grey line with yellow dots). Clinopyroxene from Klepa basalts is shown for comparison (Prelević et al., 2017). Normalizing values after Sun and McDonough (1989). (For interpretation of the references to colour in this figure legend, the reader is referred to the Web version of this article.)

resembles arc-type or orogenic type lavas with high Zr/Nb (12–13), Zr/Hf (45–46), Nb/Yb (down to 11–13) and Nb/Ta (down to 15–17) and variable La/Yb (45–48) (Table 1). They demonstrate the characteristic features of orogenic volcanic rocks in primitive-mantle normalized trace element diagram, including high LILE (including U, Th)/HFSE, high LREE/HREE, peaks at Pb and troughs at Nb, Ta and Ti, despite the fact that this signature is partially overprinted by the effects of alteration (Fig. 9), including excessive depletions in Cs, Rb, Ba and K (see green array in Fig. 9a). In a Th/Yb vs Nb/Yb diagram (Fig. 10a), the lamprophyric samples are displaced from the MORB field towards the arc lava field (Pearce, 2008).

4.4. Isotopic compositions

The leached samples of the Ripanj lamprophyres have radiogenic signatures with $^{87}Sr/^{86}Sr$ around 0.7066, and unradiogenic $^{143}Nd/^{144}Nd_i$ as low as 0.51245. Both isotopic systems show no or slight variation (Sr isotopes), which is interpreted to indicate that the Sr isotopic composition in most of the investigated samples was not affected significantly by alteration (Fig. 11a). Most probably, this is due to the storage of Sr in apatite that is quite abundant and was not affected by alteration, whereas Nd is generally not prone to be mobilized by alteration fluids. In contrast, the initial Pb isotopic composition of the Ripanj lamprophyric rocks shows considerable variation with $^{206}Pb/^{204}Pb$ in the range of 17.6–18.3 and $^{208}Pb/^{204}Pb$ in the range of 37.6–38.2. The major Pb host are feldspar minerals (K-feldspar), and their pseudomorphic replacement by albite and sericite redistributed this element. This may have resulted in variable over-correction of *in situ* Pb-growth and apparently too low calculated initial Pb isotopic compositions (Fig. 11b). Therefore, phlogopite, which has very low U/Pb and Th/Pb ratios (Table 1), was used to better constrain the initial Pb isotope signature (Fig. 11b). The data show that the phlogopite from the Ripanj lamprophyre as well as the whole-rock samples do not plot within the MORB array. The Ripanj lamprophyre samples have high $^{207}Pb/^{204}Pb$ ratios of 15.64 at relatively unradiogenic $^{206}Pb/^{204}Pb$ and fall above the OIB field (Fig. 11b).

4.5. New Ar–Ar age data

We analysed two phlogopite concentrates (TM02bts and TM02bt2) from the freshest samples of the Ripanj lamprophyric intrusion by the $^{40}Ar/^{39}Ar$ laser probe method.

The age spectra include more than 53% and 76% of total ^{39}Ar, respectively (Supplementary dataset). Both samples gave an undisturbed age spectrum with some Ar loss indicated by first steps

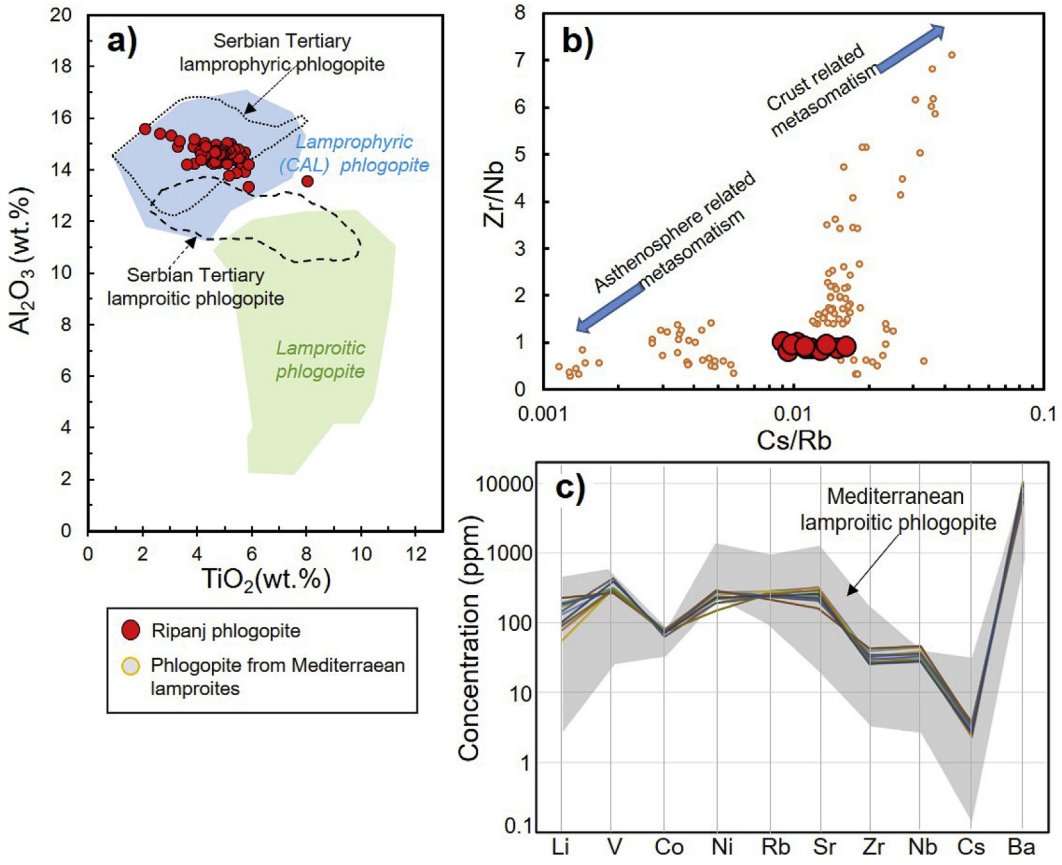

Fig. 7. a) Al_2O_3 vs TiO_2 for phlogopite from the Ripanj lamprophyre. Fields for Serbian Cenozoic lamprophyric and lamproitic phlogopite are after Prelević et al. (2005), fields for calk-alkaline (CAL) lamprophyric and lamproitic phlogopite are from Mitchell and Bergman (1991), Araujo et al. (2001) and Tappe et al. (2003). b) Trace element ratios Zr/Nb vs Cs/Rb for phlogopite from the Ripanj lamprophyre compared with phlogopite from Mediterranean lamproites (Fritschle et al., 2013). c) Multielement plots illustrating the differences between trace element concentrations (in ppm) for phlogopite in the Ripanj lamprophyre and phlogopite from Mediterranean lamproites. The figure illustrates general overlap with the lamproitic phlogopite, with Li, V, Co and Ba plotting at the most enriched end of the compositional range. Ripanj phlogopite shows significant Ni depletion relative to lamproitic phlogopite.

and some disturbance observed in the last steps. In the inverse isochron diagrams, 11 measurements out of 20 give an age around 86 Ma. In the inverse isochron diagrams, the data show a linear correlation indicating a dominant contribution from two Ar components: radiogenic Ar and atmospheric Ar. In both datasets, one intercept value gives an age of around 86 Ma. The other intercept ($^{40}Ar/^{36}Ar = 294$) is similar to the atmospheric ratio of 296 (Renne et al., 2009). The obtained age spectra do not show the complex release pattern typical for altered and some metamorphic minerals (e.g. excess Argon and thermal overprint with Ar loss), despite chloritization affected the samples with variable intensity (Supplementary dataset). This plateau indicates that phlogopite developed as a closed system since initial crystallization (closure) or complete thermal resetting. Because the analysed phlogopite contains considerable fresh portions, thermal resetting is unlikely. Therefore, the obtained age represents the crystallization age of the Ripanj lamprophyric intrusion.

In summary, the two different mineral separates yield consistent well-defined plateau ages (containing >50% of the released ^{39}Ar) of 86.6 ± 0.7 Ma and 86.5 ± 0.6 Ma (uncertainties quoted at 2 σ) (Supplementary dataset). The overlap of the two age determinations within analytical uncertainty allowed calculation of a weighted average age of 86.5 ± 0.5 Ma for emplacement of the Ripanj lamprophyre (Supplementary dataset). The new mineral-derived $^{40}Ar/^{39}Ar$ age is in excellent agreement with the stratigraphical relationships, which indicate a Early Cretaceous (Berriasian-Valanginian) age (Toljić et al., 2018). For the flysch sediments that are intruded by lamprophyre.

5. Discussion

5.1. Effects of alteration and AFC processes

Alteration minerals observed in the Ripanj Late Cretaceous lamprophyre include albite, chlorite, epidote, carbonates and pyrite. This mineral assemblage is typical for spilitization of mafic magmatic rocks. Spilitization was thorough and resulted in the pseudomorphic replacement of feldspars and subordinately clinopyroxene and phlogopite. Quantitatively, the most significant alteration process is the albitization of feldspars; while fresh plagioclase is not observed, the fresh orthoclase was found only in small amounts in the investigated samples (Fig. 4).

Pseudomorphic replacement of feldspar in spilitic rocks is the result of fluid-rock interaction related to the hydrothermal circulation of seawater (Vallance, 2018 and reference therein). Depending on the reaction history of the hydrothermal fluid, spilitic mafic rocks are enriched in Na_2O (>3–4 wt %), variably depleted in CaO, and extremely depleted in K_2O (e.g. Mottl and Holland, 1978). They have high modal albite (>20–30%) and ubiquitous epidote segregations (Clauer et al., 1985) reflecting the mobilization of Na_2O, CaO, Al_2O_3, and Fe_2O_3 by infiltrating hot seawater (Graham, 1976). Spilitization usually changes the bulk-rock K contents and results in high values for loss on ignition (LOI). Apart from variable depletion of K_2O, Ba, Cs and Rb, it also may result in a slight increase in $^{87}Sr/^{86}Sr$ (e.g., Menzies and Seyfried, 1979).

In case of the Ripanj lamprophyre samples, such intense

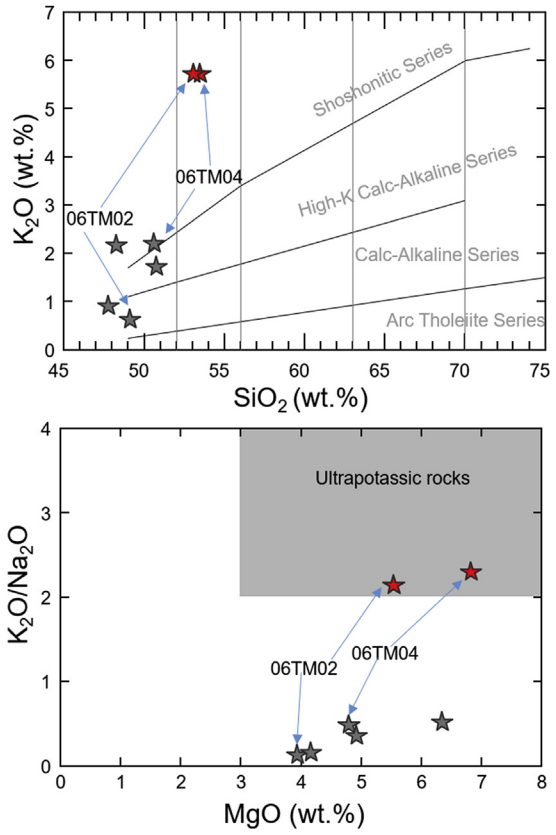

Fig. 8. a) K_2O vs SiO_2 (Peccerillo and Taylor, 1976) and b) MgO vs K_2O/Na_2O diagram for samples from the Ripanj lamprophyre. Altered whole-rock analyses of 06TM02 and 06TM04 are represented by grey stars, whereas the reconstructed values are depicted by red stars. Using the criteria of Foley et al. (1987), the reconstructed composition is ultrapotassic, with K_2O >3%, MgO >3%, and K_2O/Na_2O > 2. (For interpretation of the references to colour in this figure legend, the reader is referred to the Web version of this article.)

transformation of feldspar to albite has reduced the bulk-rock K content to less than 1 wt %, which is far less than expected for ultrapotassic rocks. However, the impact of spilitization on the geochemistry is largely restricted to the depletion of K_2O, Ba, Cs and Rb, combined with a slight variation in $^{87}Sr/^{86}Sr$ but intense variation in Pb isotopes, whereas other elements are not affected.

Moderately elevated MgO contents (4–6.4 wt % MgO) coupled with relatively low Ni and Cr concentrations (15–40 ppm and 22–35 ppm, respectively; Table 1) in all samples suggest certain extent of fractionation of the parental magmas. For sub-alkaline basalts, the primary melts in equilibrium with lherzolitic mantle will have MgO contents between 10 and 15 wt % and about 400–500 ppm Ni and 400–1100 ppm Cr (Roeder and Emslie, 1970). Primary ultrapotassic melts, which are derived from a metasomatized mantle that has been enriched in phlogopite and pyroxene (e.g. Conticelli et al., 2015; Lustrino et al., 2011; Prelević et al., 2008; Foley and Peccerillo, 1992; Foley, 1992; Foley et al., 1987), do not necessarily have comparably high MgO concentrations (8–10 wt %; Förster et al., 2018; Förster et al., 2017). Thus, the Ripanj lamprophyres with maximum of 6.4% MgO may have experienced only restricted olivine and clinopyroxene fractionation.

On the other hand, the fact that the lamprophyric magma in Ripanj had intruded into the weakly consolidated Cretaceous paraflysch, makes the assimilation of the sediments a potential mechanism responsible for potassium and trace element enrichment, and ultimately for the orogenic signature of the lamprophyre. Numerous studies on lamprophyres, lamproites and other ultrapotassic alkaline lavas, however, have convincingly excluded the possibility that assimilation of crustal material was principally responsible for the orogenic signature of these rocks (Fraser et al., 1985; Conticelli and Peccerillo, 1992). The argument used is that the trace element concentrations in the ultrapotassic lavas like lamprophyres and lamproites, including Sr, Nd and especially Pb concentrations, are more than twice those of the continental crust, implying that the elemental and isotopic compositions of the magmas were not sensitive to crustal contamination and reflect the characteristics of their source mantle. Similar argumentation is also valid for the Ripanj lamprophyre samples. Assimilation of crustal material cannot account for the orogenic geochemical fingerprints of the Ripanj lamprophyre samples (Fig. 9a), as most trace elements in the Ripanj lamprophyres have concentrations that are more than twice those of the average continental crust and the local sedimentary rocks (Fig. 9a), which makes the trace element compositions of the magmas little sensitive to crustal contamination. Thus, the trace element pattern of the Ripanj lamprophyres reflects the characteristics of their mantle source. Similarly, the Nd isotopic composition of the lamprophyres is unlikely to be affected to a significant extent by assimilation as the lamprophyres have considerably higher REE concentrations than the surrounding basement rocks. This is further supported by the considerable

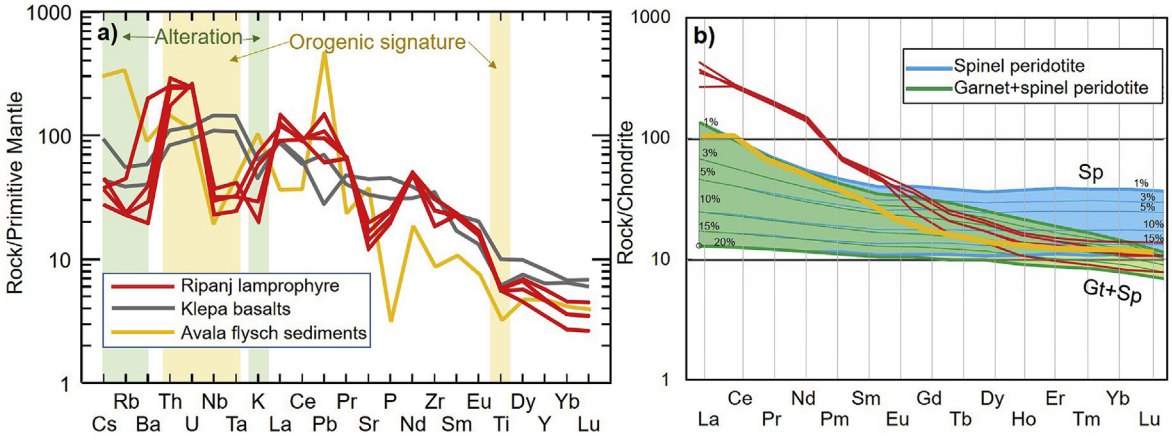

Fig. 9. a) Primitive mantle-normalized trace element variation diagram for representative samples of the Ripanj lamprophyre. Normalization after Sun and McDonough (1989). b) Chondrite-normalized REE patterns for samples of the Ripanj lamprophyre. Trajectories for, partial melts of garnet- and spinel-facies mantle are calculated using the following source mineralogy: garnet-facies harzburgite $Ol_{0.55}Opx_{0.22}Cpx_{0.18}Grt_{0.05}$ and spinel-facies harzburgite $Ol_{0.55}Opx_{0.22}Cpx_{0.18}Spl_{0.05}$. Derived partial melts are 1, 3, 5, 10, 15, 20%. Melt derived from garnet-facies (green field) and spinel-facies (blue field) cannot produce the signature of Ripanj lamprophyre sample. Normalization after Sun and McDonough (1989). (For interpretation of the references to colour in this figure legend, the reader is referred to the Web version of this article.)

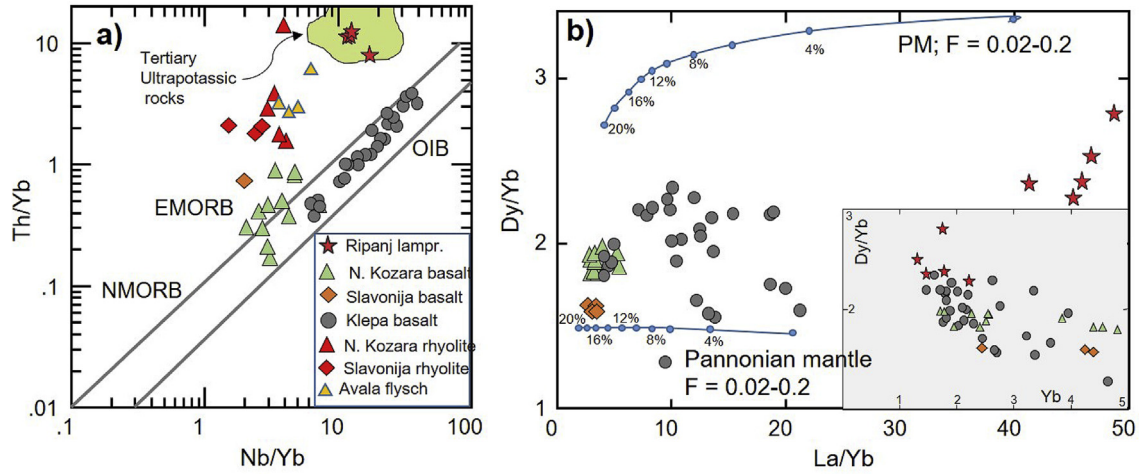

Fig. 10. a) Nb/Yb vs. Th/Yb (Pearce and Peate, 1995) diagram for the Late Cretaceous Sava-Vardar Zone basaltic volcanic rocks. Note the position of the reference field for Serbian Ultrapotassic Cenozoic lavas. b) Results of trace-element modelling of Late Cretaceous Sava-Vardar Zone basaltic volcanic rocks: La/Yb vs Dy/Yb. Modelled trajectories are for non-modal, batch partial melts (Shaw, 1970) of garnet-facies lherzolite ($Ol_{0.60}Opx_{0.25}Cpx_{0.09}Grt_{0.06}$) that melts in the proportions ($Ol_{0.12}Opx_{0.25}Cpx_{0.30}Grt_{0.33}$) and amphibole–apatite–ilmenite-lherzolite from spinel-facies mantle. Tick marks on the curves represent percentage of melt extracted (20, 18, 16, 14, 12, 10, 8, 6, 4, 2%). Source compositions: Primitive Mantle (PM) of McDonough (1990) and Pannonian metasomatized mantle of Vaselli et al. (1995).

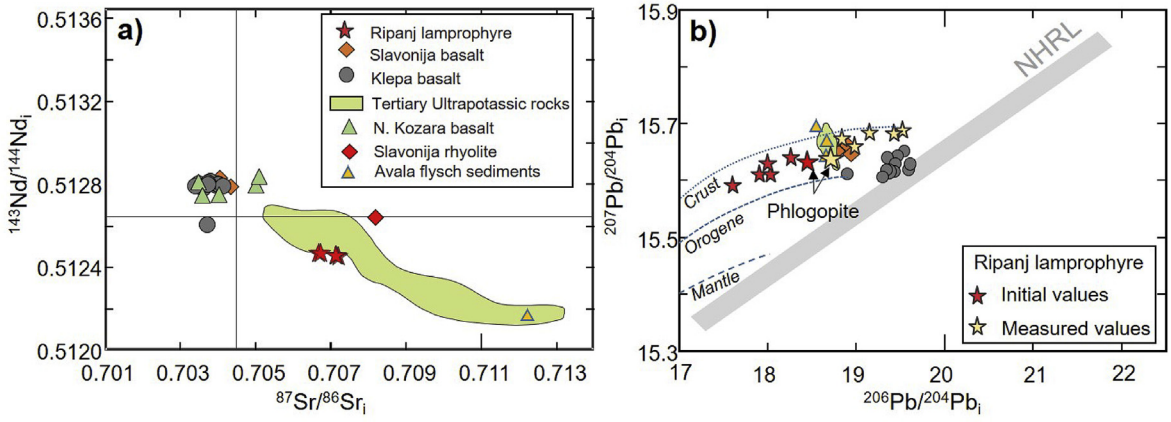

Fig. 11. a) $^{87}Sr/^{86}Sr$ vs $^{143}Nd/^{144}Nd$ and b) $^{206}Pb/^{204}Pb$ vs. $^{207}Pb/^{204}Pb$ diagrams of Ripanj lamprophyre, Papuk basalts and rhyolites (Pamić et al., 2000), Serbian Cenozoic ultrapotassic rocks and Avala flysch sediments (Prelević et al., 2005), N. Kozara basalts (Ustaszewski et al., 2009) and Klepa basalts (Prelević et al., 2017). NHRL-Northern Hemisphere Reference Line from Hart (1984). The samples with elevated $^{87}Sr/^{86}Sr$ values from Kozara (top right quadrant) are likely affected by syn- or postmagmatic alteration in contact with seawater.

difference between the Pb isotopic compositions of the lava and the basement rocks (Fig. 11b). The major component of the basement is comprised by Cretaceous sediments that have $^{207}Pb/^{204}Pb$ and $^{208}Pb/^{204}Pb$ isotopic ratios far higher than the lamprophyres.

5.2. Constraints on the mantle source of the Ripanj lamprophyric intrusion

Ultrapotassic basaltic rocks have some of the most extreme geochemical compositions among mantle-derived melts (e.g. Prelević et al., 2008 and references therein). The orogenic ultrapotassic rocks are characterized by high K_2O contents (3–12 wt %), enrichment of K_2O relative to Na_2O with K_2O/Na_2O »2 at MgO >3 wt %, extreme trace element enrichment, and crust-like Sr, Nd, and Pb isotopic compositions (Foley and Peccerillo, 1992; Prelević et al., 2008 and references therein). There are two types of models explaining the formation of the orogenic ultrapotassic basaltic rocks: (i) single stage models invoke direct sediment/crust recycling in the mantle (Campbell et al., 2014; Mallik et al., 2016; Wang et al., 2017) and (ii) two-stage models involve metasome melting (vein+wall rock model of Foley, 1992).

(i) Many recent studies propose that ultrapotassic melts form by melting of subducted sediments (Mallik et al., 2016) and/or continental crust (Wang et al., 2017) and the reaction of these melts with mantle peridotite in a single stage during subduction and collision (Campbell et al., 2014). Subducted crustal rocks have in general low solidus temperatures of ≥675 °C, which strongly depends on pressure and volatile contents (; Wang et al., 2017 and references therein). Felsic crustal material subducted to mantle depth will preferentially melt and these melts will react with the surrounding peridotite. Continental lithologies usually show K/Na of 1–2 and are K-rich compared to mantle rocks. Therefore, recycling of continental lithologies may account for the K-enrichment of mantle melts (Sekine and Wyllie, 1982). The conception of a single-stage formation of ultrapotassic lavas from recycled crustal components is based on the geochemical enrichment and the extreme isotopic signatures, resembling crustal/sedimentary lithologies, including blueschists (Tommasini et al., 2011), terrigenous siliciclastic sediments (Prelević et al., 2008), and marly sediments (Avanzinelli et al., 2008).

(ii) Metasome melting models propose that the recycling of the crustal component(s) do not necessarily have to result in volcanism, but produce intermediate lithologies in the mantle, so-called metasomes (Förster et al., 2019). The metasomes are a result of the extreme melt-mantle reaction, which severely enrich the mantle peridotite in phlogopite and pyroxene (e.g. Conticelli et al., 2015; Lustrino et al., 2011; Prelević et al., 2008). These phlogopite-rich pyroxenitic "metasomes", so-called glimmerites, are most likely formed when K-rich liquids react with peridotite to form layers and veins (Conticelli et al., 2013; Foley, 1992; Prelević et al., 2013). Experimental studies have successfully produced melts of ultrapotassic composition from phlogopite-bearing and phlogopite-veined peridotites (Förster et al., 2017 and references therein). They may melt during later processes that may be entirely unrelated to the process that formed the metasomes (Prelević et al., 2013 and references therein) as for instance mantle delamination or extension.

The whole-rock geochemistry of Ripanj lamprophyre samples demonstrate unusual trace element pattern with variable K-LILE and Ta–Nb–Ti depletion and Th–U-LREE enrichment. The depletion of LILE and potassium is directly related to low-pressure alteration resulting in the petrographically documented replacement of the original mineralogy (Figs. 3 and 4). On the other hand, the extreme enrichment in Th–U-LREE (light rare earth elements) and the depletion in Ta–Nb–Ti (Fig. 9) as well as the strontium, neodymium, and lead isotope ratios are typical signatures of the orogenic mantle. This signature resembles the signature of Cenozoic ultrapotassic lavas (Figs. 10 and 11), implying the Late Cretaceous and Cenozoic ultrapotassic rocks are derived from a mantle source that is metasomatized by recycled continental crust (Prelević et al., 2005) typical for lamproites along the Alpine-Himalayan belt (Prelević et al., 2008).

The similar geochemical character of the Late Cretaceous and Cenozoic ultrapotassic lavas implies that primary melts tapped the same lithospheric mantle source, which provides support for the metasome-melting model. The recurrence of Late Cretaceous and Cenozoic ultrapotassic volcanism in the Ripanj area (Fig. 1b) with a similar orogenic geochemical signature directly implies that the crustal signature is situated in the anciently metasomatized mantle lithosphere that has been tapped in the Late Cretaceous, Oligocene, Early Miocene, and Late Miocene. This repeated magmatic activity coincides with major tectonic changes within the region, indicating that metasomatized mantle domains may reside within the mantle lithosphere for a long time (Scarrow et al., 2011) and their episodic activation represents an integral aspect of the broader tectonic development.

5.3. Geodynamics of the Late Cretaceous volcanism along the Sava-Vardar Zone

Early Cretaceous plate reorganization in Europe was associated with the accelerated opening of the Atlantic Ocean and the broadening of the Alpine Tethys (Pieniny–Valais trough) (e.g. Dewey et al., 1988). Generally, this time is characterized by continued left lateral convergence between Europe and Africa. In the Late Cretaceous, this movement changed to a counter-clockwise rotation of Africa relative to Europe described by a new Euler pole. In the Balkans, the main movement vectors changed from E–W to more N–S and was associated with shearing along the Sava–Vardar belt and farther north along the Alcapa block (Csontos and Vörös, 2004). This reorganization resulted in the formation of a large number of NNW-SSW oriented syndepositional normal faults, indicating a change of the tectonic setting from compressional one to WSW-ENE extension. Notably, this deformation occurred at the same time as the magmatism in the Sava-Vardar Zone (Toljić et al., 2018).

Due to this reorganization, most of the terranes in central Europe were amalgamated and remaining oceanic domains of the former Tethyan ocean continued to close. The following oceanic tracts were suggested to have been open at that time: the Alpine Tethys (Pieniny–Valais) (e.g. Dewey et al., 1988), the Budva–Pindos Ocean (Csontos and Vörös, 2004), the Sava Ocean (Gallhofer et al., 2015; Schmid et al., 2008; Ustaszewski et al., 2010), and the Severin-Ceahlau Ocean (Neubauer, 2015). Importantly, the two mutually excluding models require the existence of different oceanic domains: one model invokes the survival of the Sava Ocean in the Cretaceous and the other model implies the existence of the Budva–Pindos Ocean (to thesouth of the Sava Ocean) and the Severin-Ceahlau Ocean farther to the north (Csontos and Vörös, 2004; Neubauer, 2015) (Fig. 1a). In both models, the existence of the Apuseni-Banat-Timok-Panagirište-Srednjogorje volcanic belt (ABTS), which is broadly contemporaneous with magmatism along the Sava-Vardar Zone, is instrumental in linking the Cretaceous plate movements with oceanic subduction (Fig. 1a).

Here is a short description of the key features of the two models for the geodynamic position of the Sava-Vardar Zone (Fig. 12):

i) The Sava-Vardar Zone is situated in the fore-arc region during ongoing northward subduction of the late Neotethyan Ocean (e.g. Gallhofer et al., 2015; Toljić et al., 2018) and magmatism is most likely caused by ridge subduction or slab roll-back (Fig. 12a). Such a scenario explains the broad contemporaneity of arc magmatism in the ABTS magmatic and metallogenic belt (Fig. 1a) with the near-trench magmatism in the Sava-Vardar Zone.
ii) In the Late Cretaceous, the Sava-Vardar Zone represents a diffuse tectonic boundary between the Adria block and Europe that had collided earlier with each other (e.g. Csontos and Vörös, 2004; Neubauer, 2002). This model implies that the Vardar Tethys (Neotethys) closed in the Upper Jurassic - Lower Cretaceous. Thus, the Late Cretaceous volcanism along the Sava-Vardar Zone occurred in an intracontinental setting closely associated with transtensional tectonics (Köpping et al., 2019) (Fig. 12b). In order to explain ABTS volcanic belt, this model proposes an additional oceanic tract farther to the east, the so-called Severin-Ceahlau ocean (Fig. 1a) that represents a Middle to Late Jurassic narrow oceanic basin (Neubauer, 2002, 2015) similar to the Alpine Tethys. Arc magmatism in the ABTS belt would be related to the subduction of "Severin-Ceahlau" oceanic realm beneath the Carpatho-Balkanides, whereas magmatism and sedimentation in the Sava-Vardar Zone would be related to the extension in the back-arc (or roll-back).

5.4. Petrogenesis of the Late Cretaceous volcanism along the Sava-Vardar Zone

Late Cretaceous magmatism along the Sava-Vardar Zone includes several centres of small-volume transitional to alkaline Na-basalt (with subordinate rhyolitic rocks) and rare ultrapotassic basalts (Fig. 1a) (Pamić et al., 2000; Ustaszewski et al., 2009; Cvetković et al., 2014; Prelević et al., 2017) The geochemical and isotope compositions of the Late Cretaceous lavas (Figs. 9–11) suggest that all these volcanic rocks are not derived from dismembered ophiolite sequences (see Prelević et al., 2017), but represent intracontinental magmas derived from variably enriched mantle sources. Most lava occurrences (Klepa, Kozara, Slavonija) are transitional to Na-alkaline basalts showing a clear "within plate" geochemical signature with typical mantle-like $^{87}Sr/^{86}Sr_i$, $^{143}Nd/^{144}Nd_i$ and $^{206}Pb/^{204}Pb_i$ ratios (Fig. 11) with relatively high

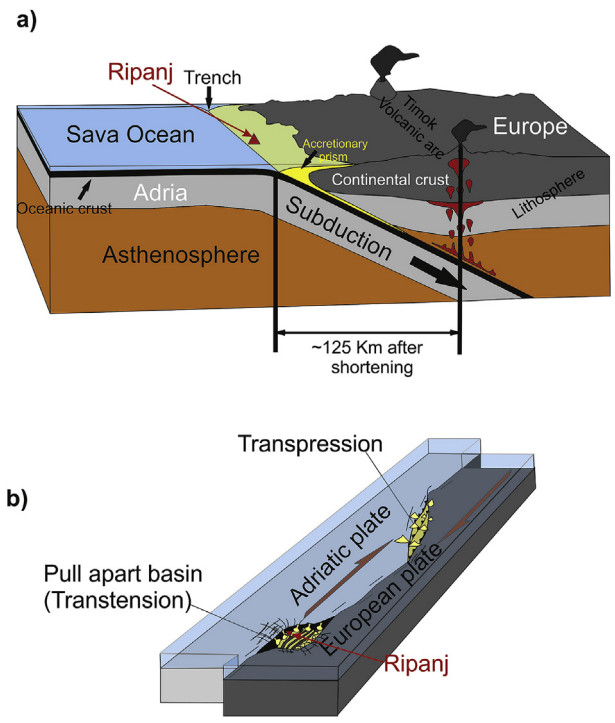

Fig. 12. Two viable but mutually-excluding geodynamic scenarios for the Late Cretaceous magmatism in the Balkans: a) The Sava-Vardar ocean still existed in the Late Cretaceous and was subducted under the European plate (Gallhofer et al., 2015; Schmid et al., 2008; Ustaszewski et al., 2009). In this scenario, the subduction produced the Late Cretaceous Apuseni-Banat–Timok–Srednjegorje magmatic arc (Gallhofer et al., 2015). The Sava-Vardar Zone represents a fore-arc region (Toljić et al., 2018) and the magmatism is triggered by the ridge subduction. b) Alternatively, the magmatism within the Sava-Vardar Zone is intracontinental and related to transtensional tectonics along the suture between Adria block represented by Dinarides (a distal paleogeographic domain) and European plates that collided earlier in Late Jurassic.

HFSE/LILE ratios, and without orogenic geochemical signatures such as high LILE/HFSE ratios, positive Pb and negative Ti–Nb–Ta anomalies. A broad range of MREE/HREE ratios in these locations suggests polybaric mantle melting (Fig. 10). Melting models demonstrate that the mafic melts most probably were generated as a continuum with low-degree melting in the asthenospheric mantle within the garnet stability field and high-degree melting of the freshly metasomatized lithospheric mantle in the spinel stability field (Prelević et al., 2017). The presence of transitional to Na-alkaline basalts in these locations implies a large range of partial melting degree variation from 5 to 25%, which may be produced by variation in extension (Prelević et al., 2017). In contrast, the Ripanj lamprophyre that is the oldest Late Cretaceous activity, is unique in showing an orogenic signature. This metasomatic signature is derived from the mantle lithosphere that has been geochemically modified during previous subduction event(s), definitely prior to the formation of the Sava-Vardar Zone. The orogenic signature is most probably stored in the metasomatic domains comprised of phlogopite-pyroxenites (Förster et al., 2019) when the subducted sediments are consumed during interaction with surrounding mantle peridotite.

The ultimate trigger of the mantle melting along the Sava-Vardar Zone should be localized extension during transtensional tectonics, probably in a system of pull-apart basins (Köpping et al., 2019). A direct response to the extension could be the incursion of fresh asthenospheric mantle beneath the thinning lithosphere and partial melting of the mantle. Melting started with low degrees of decompression melting of the sublithospheric mantle and was followed by increasingly more important melting of the metasomatized lithospheric mantle. This change of the magma source resulted in a general transition of the chemical signature from orogenic to within-plate type, as a result of the heterogeneity of the lithospheric mantle. Variations in lithosphere thickness and thermal structure across the Sava-Vardar Zone may have amplified transient geochemical variation related to the depth of the melt segregation (MREE/HREE variation; Fig. 10b).

Geochemistry offers no further insights into the details of the geodynamic position of the Sava-Vardar-Zone with respect to the geotectonic models presented above; our inferences define this magmatic belt as intracontinental, heterogeneous and related to transtension (Köpping et al., 2019). The lamprophyric magmatism in Ripanj at 87 Ma constrains the onset of this transtensional tectonics in the Balkans much earlier than previously proposed on basis of post-Oligocene lacustrine sediments (Marović et al., 2000). This earlier onset agrees well with the general observation that lamprophyres represent tectonomagmatic time marker for changes in the geodynamic conditions (Scarrow et al., 2011).

5.5. Recurrent ultrapotassic volcanism in the Balkans

There are three episodes of low-volume mafic ultrapotassic magmatism within the Sava-Vardar Zone that are related to (i) Cretaceous transtensional tectonics (Prelević et al., 2017), (ii) Oligocene-Early Miocene orogenic collapse of the Dinarides and the Pannonian Basin, and (iii) Late Miocene orogenic collapse within the Aegean (Cvetković et al., 2004, 2016; Prelević et al., 2005). The Cretaceous ultrapotassic magmatism is rare and scattered. The Cenozoic magmatic episodes are more voluminous and include, apart from the sporadic occurrences of ultrapotassic and high-K calk-alkaline basaltic and andesitic lavas, also major granitic and granodioritic plutons (Cvetković et al., 2004, 2016; Prelević et al., 2005 and references therein). The Oligocene-Early Miocene episode predominates in the northern part of the Sava-Vardar Zone, whereas the Late Miocene episode predominates in the southern part, mostly in North Macedonia (Fig. 1a).

The occurrence of Ripanj lamprophyric sill demonstrates recurrent ultrapotassic magmatism along the Sava-Vardar Zone back to the Cretaceous. Given the isotopic and geochemical composition of post-collisional lavas in orogenic areas like the Alpine-Himalayan belt, which show high $^{87}Sr/^{86}Sr$ and trace element pattern similar to the average composition of the regional upper crust (Prelević et al., 2008), the recycling of the material derived from the upper crust would be the most viable mechanism for the metasomatism of the source of the Ripanj ultrapotassic rocks. The timing of this recycling, however, is an open issue that is hard to be constrained (Tommasini et al., 2011). The fact that ultrapotassic lavas occur in a number of scattered localities in different tectono-magmatic episodes may serve to characterize the mantle composition under the Sava-Vardar Zone adding considerably to our understanding of the origin and evolution of the crustally metasomatized lithospheric mantle. Our basic assumption here is that both Cretaceous and Cenozoic ultrapotassic lavas are likely derived from the same previously metasomatized lithospheric mantle, as is indicated by (i) the resemblance of their trace element and isotopic signature (Figs. 10 and 11) and (ii) their Pb isotopic composition that falls on the same lead isotope growth curve between crust and orogene (Zartman and Doe, 1981, Fig. 11b); this is further supported by Fig. 13.

In Fig. 13 we use the initial $^{206}Pb/^{204}Pb$ ratio of the Ripanj lamprophyre and Cenozoic ultrapotassic lavas, which differs because of the contrasting age, to model the μ ($^{238}U/^{204}Pb$) ratio of their metasomatized mantle source. As the Pb isotopic composition of the Ripanj whole-rock samples is characterized by considerable scatter due to alteration and related overcorrection of *in situ*

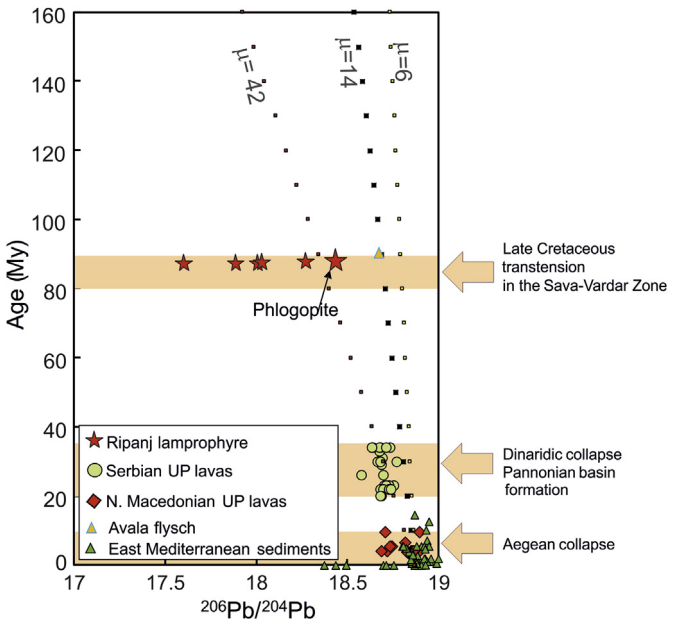

Fig. 13. Geochemical characteristics of Ripanj lamprophyric rocks in time and space. Besides ultrapotassic rocks of different ages including Late Cretaceous Ripanj lavas, Serbian and North Macedonian Cenozoic ultrapotassic lavas for comparison, we plot sediments that represent a potential source of the crustal material recycled in the mantle through subduction process. These sediments should convey crust-like geochemical signature to the mantle source of the ultrapotassic lavas (see text). Data sources: Avala flysch (Prelević et al., 2005), Mediterranean sediments (Klaver et al., 2015; Rodrigo-Gámiz et al., 2015), Serbian UP lavas and N. Macedonian UP lavas (Prelević et al., 2005, 2008).

growth, the initial Pb isotopic signature of the Ripanj source is taken to correspond most closely to the Pb isotopic composition of fresh phlogopite phenocrysts (Table 1). We also plot recent East Mediterranean sediments (Klaver et al., 2015; Rodrigo-Gámiz et al., 2015). In order to estimate the μ ($^{238}U/^{204}Pb$) of the metasomatized mantle, we traced back the composition of recent East Mediterranean sediments to 160 Ma using different μ values (Fig. 13). The $^{206}Pb/^{204}Pb$ evolution lines are modelled with μ values of the upper crust and Cretaceous sediment from the Sava-Vardar zone, in order to fit array demonstrated by Cretaceous and Cenozoic ultrapotassic lavas. The slope of the evolution model shows that the modelled Cretaceous composition of the average East Mediterranean sediment would plot on considerably more radiogenic space due to the upper-crust like μ values as low as 6 (Fig. 13), similar to Cretaceous sediments from the basement of the Ripanj lamprophyres in the uranogenic diagram with the μ values around 14. If the Late Cretaceous (phlogopite) and Cenozoic ultrapotassic lavas are derived from the same source, the contrasting Pb isotopic composition requires a mantle source with considerably higher μ values around 42 (Fig. 13).

6. Conclusions

The main findings of this study are as follows.

1. Ultrapotassic lamprophyric volcanism occurred during the Late Cretaceous in the Sava-Vardar Zone of the Balkan Peninsula. This volcanism represents the oldest manifestation of the Late Cretaceous low volume volcanism within this zone.
2. Spilitisation of the lamprophyric rocks caused K-loss and Na-addition, complicating their classification as ultrapotassic rocks. Using the original ultrapotassic modal mineralogy [e.g. abundant orthoclase and phlogopite], the pre-spilitic chemical composition was reconstructed to have K_2O > 5.5%, MgO >6%, and K_2O/Na_2O > 2.
3. The geochemical and isotopic characteristics of the originally ultrapotassic rocks can be evaluated as features of the magmatic source as a wide range of elements behaved immobile during alteration and the magmas did not undergo significant crustal contamination.
4. The Ripanj lamprophyric rocks are derived from the metasomatized lithospheric mantle that ultimately originated from the recycling of old continental crust or its sedimentary derivatives. Comparison with other volcanic occurrences along the Sava-zone demonstrated that the lithospheric mantle was heterogeneous owing to regionally different metasomatic processes.

Acknowledgements

This work was supported through the Deutsche Forschungsgemeinschaft (DFG) within the project BA 3441/1 and 2 and Serbian Ministry of Education, Science and Technological Development, Grant/Award Number: 176016. We would like to thank B. Hübner and H. Rothe (both GFZ) for help with sample leaching, ion-exchange chromatography and trace element analysis. The authors also thank to SEM–EDS laboratory of the University of Belgrade-Faculty of Mining and Geology for support. Finally, we are gratefulto Prof. Franc Neubauer and one anonymous reviewer for reading one of the earlier versions of the manuscript, and Prof. Michael Roden for handling our manuscript.

Appendix A. Supplementary data

Supplementary data to this article can be found online at https://doi.org/10.1016/j.lithos.2019.105268.

References

Araujo, A.L.N., Carlson, R.W., Gaspar, J.C., Bizzi, L.A., 2001. Petrology of kamafugites and kimberlites from the alto paranaıba alkaline province, minas gerais, Brazil. Contrib. Mineral. Petrol. 142, 163–177.
Avanzinelli, R., Elliott, T., Tommasini, S., Conticelli, S., 2008. Constraints on the genesis of potassium-rich Italian volcanic rocks from U/Th disequilibrium. J. Petrol. 49, 195–223.
Božović, M., Prelević, D., Romer, R.L., Barth, M., Van den Bogaard, P., Boev, B., 2013. The demir kapija ophiolite, Macedonia (FYROM): a snapshot of subduction initiation within a back-arc. J. Petrol. 54, 1427–1453.
Campbell, I.H., Stepanov, A.S., Liang, H.-Y., Allen, C.M., Norman, M.D., Zhang, Y.-Q., Xie, Y.-W., 2014. The origin of shoshonites: new insights from the Tertiary high-potassium intrusions of eastern Tibet. Contrib. Mineral. Petrol. 167, 983.
Clauer, N., Vidal, P., Auvray, B., 1985. Differential behavior of the Rb-Sr and K-Ar systems of spilitic flows and interbedded metasediments - the spilite group of Erquy (Brittany, France) - paleomagnetic implications. Contrib. Mineral. Petrol. 89, 81–89.
Conticelli, S., Peccerillo, A., 1992. Petrology and geochemistry of potassic and ultrapotassic volcanism in central Italy: petrogenesis and inferences on the evolution of the mantle sources. Lithos 28, 221–240.
Conticelli, S., Avanzinelli, R., Poli, G., Braschi, E., Giordano, G., 2013. Shift from lamproite-like to leucititic rocks: Sr–Nd–Pb isotope data from the Monte Cimino volcanic complex vs the Vico stratovolcano, Central Italy. Chem. Geol. 353, 246–266.
Conticelli, S., Boari, E., Burlamacchi, L., Cifelli, F., Moscardi, F., Laurenzi, M.A., Ferrari Pedraglio, L., Francalanci, L., Benvenuti, M.G., Braschi, E., Manetti, P., 2015. Geochemistry and Sr-Nd-Pb isotopes of Monte Amiata Volcano, Central Italy: evidence for magma mixing between high-K calc-alkaline and leucititic mantlederived magmas. Ital. J. Geosci. 134, 268–292.
Csontos, L., Vörös, A., 2004. Mesozoic plate tectonic reconstruction of the Carpathian region. Palaeogeogr. Palaeoclimatol. Palaeoecol. 210, 1–56.
Cvetković, V., Downes, H., Hock, V., Prelević, D., Lazarov, M., 2010. Mafic alkaline metasomatism in the lithosphere underneath East Serbia: evidence from the study of xenoliths and the host alkali basalts. Geological Society, London, Special Publications 337, 213–239.
Cvetković, V., Prelević, D., Downes, H., Jovanović, M., Vaselli, O., Pecskay, Z., 2004. Origin and geodynarnic significance of Tertiary postcollisional basaltic magmatism in Serbia (central Balkan Peninsula). Lithos 73, 161–186.
Cvetković, V., Prelević, D., Schmid, S., 2016. Geology of south-eastern Europe. In: Papić, P. (Ed.), Mineral and Thermal Waters of Southeastern Europe. Springer International Publishing, Cham, pp. 1–29.

Cvetković, V., Šarić, K., Grubić, A., Cvijić, R., Milošević, A., 2014. The Upper Cretaceous Ophiolite of North Kozara – Remnants of an Anomalous Mid-ocean Ridge Segment of the Neotethys? Geologica Carpathica, p. 117.
Dalrymple, G.B., Duffield, W.A., 1988. High precision 40Ar/39Ar dating of Oligocene tephra from the Mogollon–Datil volcanic field using a continuous laser system. Geophys. Res. Lett. 15, 463–466.
Deer, W.A., Howie, R.A., Zussman, J., 1966. An Introduction to the Rock Forming Minerals. Longmans, Green and Co., London, p. 528.
Dewey, J.F., 1988. Extensional Collapse of Orogens. Tectonics 7, pp. 1123–1139.
Foley, S., Peccerillo, A., 1992. Potassic and ultrapotassic magmas and their origin. Lithos 28, 181.
Foley, S.F., 1992. Vein-plus-wall-rock melting mechanisms in the lithosphere and the origin of potassic alkaline magmas. Lithos 28, 435–453.
Foley, S.F., Venturelli, G., Green, D.H., Toscani, L., 1987. The ultrapotassic rocks: characteristics, classification and constraints for petrogenetic models. Earth Sci. Rev. 24, 81–134.
Förster, M.W., Prelević, D., Buhre, S., Mertz-Kraus, R., Foley, S.F., 2019. An experimental study of the role of partial melts of sediments versus mantle melts in the sources of potassic magmatism. J. Asian Earth Sci. 177, 76–88.
Förster, M.W., Prelević, D., Schmück, H.R., Buhre, S., Marschall, H.R., Mertz-Kraus, R., Jacob, D.E., 2018. Melting phlogopite-rich MARID: lamproites and the role of alkalis in olivine-liquid Ni-partitioning. Chem. Geol. 476, 429–440.
Förster, M.W., Prelević, D., Schmuck, H.R., Buhre, S., Veter, M., Mertz-Kraus, R., Foley, S.F., Jacob, D.E., 2017. Melting and dynamic metasomatism of mixed harzburgite plus glimmerite mantle source: implications for the genesis of orogenic potassic magmas. Chem. Geol. 455, 182–191.
Fraser, K., Hawkesworth, C., Erlank, A., Mitchell, R., Scott- Smith, B., 1985. Sr, Nd and Pb isotope and minor element geochemistry of lamproites and kimberlites. Earth Planet. Sci. Lett. 76, 57–70.
Fritschle, T., Prelević, D., Foley, S.F., Jacob, D.E., 2013. Petrological characterization of the mantle source of Mediterranean lamproites: indications from major and trace elements of phlogopite. Chem. Geol. 353, 267–279.
Gallhofer, D., Quadt, A.v., Peytcheva, I., Schmid, S.M., Heinrich, C.A., 2015. Tectonic, magmatic, and metallogenic evolution of the Late Cretaceous arc in the Carpathian-Balkan orogen. Tectonics 34, 1813–1836.
Graham, C.M., 1976. Petrochemistry and tectonic significance of Dalradian metabasaltic rocks of the SW. Scottish Highlands. J. Geol. Soc. 132, 61–84.
Hart, S.R., 1984. A large-scale isotope anomaly in the Southern Hemisphere mantle. Science 309, 753–757.
Karamata, S., 2006. The geological development of the Balkan Peninsula related to the approach, collision and compression of Gondwanan and Eurasian units. In: Robertson, A.H.F., Mountrakis, D. (Eds.), Tectonic Development of the Eastern Mediterranean Region. Geol. Soc. Spec. Publ., Geol. Soc., London, pp. 155–178.
Klaver, M., Djuly, T., de Graaf, S., Sakes, A., Wijbrans, J., Davies, G., Vroon, P., 2015. Temporal and spatial variations in provenance of eastern mediterranean sea sediments: implications for aegean and aeolian arc volcanism. Geochem. Cosmochim. Acta 153, 149–168.
Köpping, J., Peternell, M., Prelević, D., Rutte, D., 2019. Cretaceous tectonic evolution of the Sava-Klepa Massif, Republic of North Macedonia – results from calcite twin based automated paleostress analysis. Tectonophysics 758. https://doi.org/10.1016/j.tecto.2019.03.010.
Kossmat, F., 1924. Geologie der zentralen Balkanhalbinsel—kriegsschauplaetze 1914–1918. Geologisch dargestellt 12, 1–198.
Kretz, R., 1983. Symbols for rock-forming minerals. Am. Mineral. 68, 277–279.
Le Maitre, R.W., 2002. Igneous Rocks: A Classification and Glossary of Terms: Recommendations of the International Union of Geological Sciences Subcommission on the Systematics of Igneous Rocks, 2 ed. Cambridge University Press, Cambridge, p. 236.
Lustrino, M., Duggen, S., Rosenberg, C.L., 2011. The Central– Western Mediterranean: anomalous igneous activity in an anomalous collisional tectonic setting. Earth Sci. Rev. 104, 1–40.
Mallik, A., Dasgupta, R., Tsuno, K., Nelson, J., 2016. Effects of water, depth and temperature on partial melting of mantle-wedge fluxed by hydrous sediment-melt in subduction zones. Geochem. Cosmochim. Acta 195, 226–243.
Marović, M., Djoković, I., Pešić, L., Toljić, M., Gerzina, N., 2000. The genesis and geodynamics of Cenozoic sedimentation provinces of the central Balkan Peninsula. Geotectonics 34, 415–427.
McDonough, W.F., 1990. Constraints on the composition of the continental lithospheric mantle. Earth Planet. Sci. Lett. 101, 1–18.
Mitchell, R.H., Bergman, S.C., 1991. Petrology of Lamproites. Plenum, New York.
Mottl, M.J., Holland, H.D., 1978. Chemical exchange during hydrothermal alteration of basalt by seawater—I. Experimental results for major and minor components of seawater. Geochem. Cosmochim. Acta 42, 1103–1115.
Morimoto, N., 1988. Nomenclature of pyroxenes. Mineral. Petrol. 39, 55–76.
Menzies, M., Seyfried Jr., W.E., 1979. Basalt-seawater interaction: trace element and strontium isotopic variations in experimentally altered glassy basalt. Earth Planet. Sci. Lett. 44, 463–472.
Nédli, Zsuzsanna, Tóth, Tivadar, M., Downes, Hilary, Császár, Géza, Beard, Andrew, Szabo, Csaba, 2010. Petrology and geodynamical interpretation of mantle xenoliths from Late Cretaceous lamprophyres, Villány Mts (S Hungary). Tectonophysics 489, 43–54. https://doi.org/10.1016/j.tecto.2010.03.013.
Nédli, Z.S., Tóth, T.M., 2007. Origin and geotectonic significance of upper cretaceous lamprophyres from the Villány Mts (S Hungary). Mineral. Petrol. 90, 73–107.
Nehring, F., Jacob, D.E., Barth, M.G., Foley, S.F., 2008. Laser-ablation ICP-MS analysis of siliceous rock glasses fused on an iridium strip heater using MgO dilution. Microchimica Acta 160 (Issue 1–2), 153–163.
Neubauer, F., 2002. Contrasting late cretaceous with neogene ore provinces in the alpine-balkan-carpathian-dinaride collision belt. Geological Society, London, Special Publications 204, 81–102.
Neubauer, F., 2015. Cretaceous tectonics in Eastern alps, Carpathians and dinarides: two-step microplate collision and Andean-type magmatic arc associated with orogenic collapse. Rendiconti Online Societa Geologica Italiana 37, 40–43.
Pamić, J., Šparica, M., 1983. The age of the volcanic rocks of Požeška Gora (Croatia, Yugoslavia). Radovi Jugoslavenske Akademije Znanosti i Umjetnosti 404, 183–198.
Pamić, J., Belak, M., Bullen, T.D., Lanphere, M.A., McKee, E.H., 2000. Geochemistry and geodynamics of a late cretaceous bimodal volcanic association from the southern part of the Pannonian Basin in Slavonija (northern Croatia). Mineral. Petrol. 68, 271–296.
Pamić, J., Šiparica, M., 1988. Badenian volcanics from Mt. Dilj in Slavonija (northern Croatia, Yugoslavia). Bulletin Académie des Serbe des Sciences et des Arts, Classe des Sciences Mathématiques et naturelles, Sciences naturelles XCV 47–56.
Pearce, J.A., Peate, D.W., 1995. Tectonic implications of the composition of volcanic arc magmas. Annu. Rev. Earth Planet Sci. 23, 251–285.
Pearce, J.A., Bender, J.F., DeLong, S.E., Kidd, W.S.F., Low, P.J., et al., 1990. Genesis of collision volcanism in eastern Anatolia, Turkey. J. Volcanol. Geotherm. Res. 44, 184–229.
Pearce, J.A., 2008. Geochemical fingerprinting of oceanic basalts with applications to ophiolite classification and the search for Archean oceanic crust. Lithos 100, 14–48.
Peccerillo, A., Taylor, S.R., 1976. Geochemistry of Eocene calc-alkaline volcanic rocks from the Kastamonu area, Northern Turkey. Contrib. Mineral. Petrol. 58, 63–81.
Perini, G., Conticelli, S., 2002. Crystallization conditions of leucitebearing magmas and their implications on the magmatological evolution of ultrapotassic magmas: the Vico Volcano, Central Italy. Mineral. Petrol. 74, 253–276.
Pilet, S., 2015. Generation of low-silica alkaline lavas: petrological constraints, models, and thermal implications. In: Foulger, G.R., Lustrino, M., King, S.D. (Eds.), The Interdisciplinary Earth: A Volume in Honor of Don L. Anderson, vol. 71. Geological Society of America Special Paper 514 and American Geophysical Union Special Publication, pp. 281–304.
Prelević, D., Wehrheim, S., Reutter, M., Romer, R.L., Boev, B., Božović, M., van den Bogaard, P., Cvetković, V., Schmid, S.M., 2017. The late cretaceous Klepa basalts in Macedonia (FYROM)—constraints on the final stage of Tethys closure in the Balkans. Terra. Nova 29, 145–153.
Prelević, D., Brügmann, G., Barth, M., Božović, M., Cvetković, V., Foley, S.F., Maksimović, Z., 2015. Os-isotope constraints on the dynamics of orogenic mantle: the case of the Central Balkans. Gondwana Res. 27, 1560–1573.
Prelević, D., Jacob, D.E., Foley, S.F., 2013. Recycling plus: a new recipe for the formation of Alpine-Himalayan orogenic mantle lithosphere. Earth Planet. Sci. Lett. 362, 187–197.
Prelević, D., Foley, S.F., Romer, R., Conticelli, S., 2008. Mediterranean Tertiary lamproites derived from multiple source components in postcollisional geodynamics. Geochem. Cosmochim. Acta 72, 2125–2156.
Prelević, D., Foley, S.F., Romer, R.L., Cvetković, V., Downes, H., 2005. Tertiary ultrapotassic volcanism in Serbia: constraints on petrogenesis and mantle source characteristics. J. Petrol. 46, 1443–1487.
Renne, P.R., Deino, A.L., Hames, W.E., Heizler, M.T., Hemming, S.R., Hodges, K.V., Koppers, A.A.P., Mark, D.F., Morgan, L.E., Phillips, D., Singer, B.S., Turrin, B.D., Villa, I.M., Villeneuve, M., Wijbrans, J.R., 2009. Data reporting norms for 40Ar/39Ar geochronology. Quat. Geochronol. 4, 346–352.
Rodrigo-Gámiz, M., Martínez-Ruiz, F., Chiaradia, M., Jiménez-Espejo, F.J., Ariztegui, D., 2015. Radiogenic isotopes for deciphering terrigenous input provenance in the western Mediterranean. Chem. Geol. 410, 237–250.
Rock, N.M.S., 1991. Lamprophyres. Blackie, Glasgow, p. 285.
Roeder, P., Emslie, R., 1970. Olivine–liquid equilibrium. Contrib. Mineral. Petrol. 29, 275–289.
Romer, R.L., Foerster, H.J., Breitkreuz, C., 2001. Intracontinental extensional magmatism with a subduction fingerprint; the Late Carboniferous Halle volcanic complex (Germany). Contrib. Mineral. Petrol. 141, 201–221.
Rosenbaum, G., Mo, W., 2011. Tectonic and magmatic responses to the subduction of high bathymetric relief. Gondwana Res. 19, 571–582.
Scarrow, J.H., Molina, J.F., Bea, F., Montero, P., Vaughan, A.P.M., 2011. Lamprophyre dikes as tectonic markers of late orogenic transtension timing and kinematics: a case study from the Central Iberian Zone. Tectonics 30 (4), TC4007. https://doi.org/10.1029/2010TC002755.
Schmid, S., Bernoulli, D., Fügenschuh, B., Matenco, L., Schefer, S., Schuster, R., Tischler, M., Ustaszewski, K., 2008. The Alpine-Carpathian-Dinaridic orogenic system: correlation and evolution of tectonic units. Swiss J. Geosci. 101, 139–183.
Sekine, T., Wyllie, P.J., 1982. Phase relationships in the system KAlSiO4-Mg2SiO4-SiO2-H_2O as a model for hybridization between hydrous siliceous melts and peridotite. Contrib. Mineral. Petrol. 79, 368–374.
Shaw, D.M., 1970. Trace element fractionation during anatexis. Geochem. Cosmochim. Acta 34, 237–243.
Starijaš, B., Gerdes, A., Balen, D., Tibljaš, D., Finger, F., 2010. The Moslavačka Gora crystalline massif in Croatia: a Cretaceous heat dome within remnant Ordovician granitoid crust. Swiss J. Geosci. 103, 61–82.
Stoll, B., Jochum, K.P., Herwig, K., Amini, M., Flanz, M., Kreuzburg, B., Kuzmin, D., Willbold, M., Enzweiler, J., 2008. An automated iridium-strip heater for LA-ICP-MS bulk analysis of geological samples. Geostand. Geoanal. Res. 32, 5–26.
Sun, S.S., McDonough, W.F., 1989. Chemical and isotopic systematics of oceanic

basalts; implications for mantle composition and processes. In: Saunders, A.D., Norry, M.J. (Eds.), Magmatism in the Ocean Basins. Geological Society of London, London, United Kingdom, pp. 313–345.
Tappe, S., Foley, S.F., Pearson, D.G., 2003. The Kamafugites of Uganda: a mineralogical and geochemical comparison with their Italian and Brazilian analogues. Period. Mineral. 72, 51–77.
Toljić, M., Matenco, L., Stojadinović, U., Willingshofer, E., Ljubović-Obradović, D., 2018. Understanding fossil fore-arc basins: inferences from the cretaceous adria-europe convergence in the NE dinarides. Global and Planetary Change.
Tommasini, S., Conticelli, S., Avanzinelli, R., 2011. The Th/La and Sm/La conundrum of the Tethyan realm lamproites. Earth Planet. Sci. Lett. 301, 469–478.
Ustaszewski, K., Kounov, A., Schmid, S.M., Schaltegger, U., Krenn, E., Frank, W., Fügenschuh, B., 2010. Evolution of the Adria-Europe plate boundary in the northern Dinarides: from continent-continent collision to back-arc extension. Tectonics 29 (n/a-n/a).
Ustaszewski, K., Schmid, S.M., Lugović, B., Schuster, R., Schaltegger, U., Bernoulli, D., Hottinger, L., Kounov, A., Fügenschuh, B., Schefer, S., 2009. Late Cretaceous intra-oceanic magmatism in the internal Dinarides (northern Bosnia and Herzegovina): implications for the collision of the Adriatic and European plates. Lithos 108, 106–125.
Vallance, T.G., 2018. On the chemistry of pillow lavas and the origin of spilites. Mineral. Mag. J. Mineral Soc. 34, 471–481.
Van den Bogaard, P., 1995. $^{40}Ar/^{39}Ar$ ages of sanidine phenocrysts from Laacher See tephra (12,900 yr BP): chronostratigraphic and petrological significance. Earth Planet. Sci. Lett. 133, 163–174.
Vaselli, O., Downes, H., Thirlwall, M.F., Dobosi, G., Coradossi, N., Seghedi, I., Szakacs, A., Vannucci, R., 1995. Ultramafic xenoliths in Plio-Pleistocene alkali basalts from the eastern Transylvanian Basin; depleted mantle enriched by vein metasomatism. J. Petrol. 36, 23–53.
Vasković, N., 1990. Petrological Characteristics of Tertiary Magmatism and Contact Metamorphism of Avala. University of Belgrade, Serbia, p. 258.
Wang, Y., Foley, S.F., Prelević, D., 2017. Potassium-rich magmatism from a phlogopite-free source. Geology 45, 467–470.
Zartman, R., Doe, B.R., 1981. Plumbotectonics - the model. Tectonophysics 75, 135–162.